Article

Cell

Uridylation by TUT4 and TUT7 Marks mRNA for Degradation

Jaechul Lim,[1,2,4] Minju Ha,[1,2,4] Hyeshik Chang,[1,2,4] S. Chul Kwon,[1,2] Dhirendra K. Simanshu,[3] Dinshaw J. Patel,[3] and V. Narry Kim[1,2,*]

[1]Center for RNA Research, Institute for Basic Science, Seoul 151-742, Korea
[2]School of Biological Sciences, Seoul National University, Seoul 151-742, Korea
[3]Structural Biology Program, Memorial Sloan-Kettering Cancer Center, New York, NY 10065, USA
[4]Co-first author
*Correspondence: narrykim@snu.ac.kr
http://dx.doi.org/10.1016/j.cell.2014.10.055

SUMMARY

Uridylation occurs pervasively on mRNAs, yet its mechanism and significance remain unknown. By applying TAIL-seq, we identify TUT4 and TUT7 (TUT4/7), also known as ZCCHC11 and ZCCHC6, respectively, as mRNA uridylation enzymes. Uridylation readily occurs on deadenylated mRNAs in cells. Consistently, purified TUT4/7 selectively recognize and uridylate RNAs with short A-tails (less than ~25 nt) in vitro. PABPC1 antagonizes uridylation of polyadenylated mRNAs, contributing to the specificity for short A-tails. In cells depleted of TUT4/7, the vast majority of mRNAs lose the oligo-U-tails, and their half-lives are extended. Suppression of mRNA decay factors leads to the accumulation of oligo-uridylated mRNAs. In line with this, microRNA induces uridylation of its targets, and TUT4/7 are required for enhanced decay of microRNA targets. Our study explains the mechanism underlying selective uridylation of deadenylated mRNAs and demonstrates a fundamental role of oligo-U-tail as a molecular mark for global mRNA decay.

INTRODUCTION

RNA tailing (nontemplated nucleotide addition to the 3′ end of RNA) is one of the most frequent types of RNA modification, with a deep evolutionary root and diverse molecular functions. In bacteria, adenylation of mRNA triggers RNA degradation whereas polyadenylation in eukaryotes increases the stability and translatability of mRNA (Dreyfus and Régnier, 2002). Tailing is catalyzed by a group of template-independent ribonucleotidyl transferases that contain DNA polymerase β-like nucleotidyl transferase domain (Aravind and Koonin, 1999). Apart from canonical poly(A) polymerases (PAPs) that generate poly(A) tail of mRNA, many noncanonical PAPs have been described from fission yeast to human (Martin and Keller, 2007; Norbury, 2013). Because some noncanonical PAPs catalyze uridylation instead of adenylation, noncanonical PAPs are also called terminal uridylyl transferases (TUTases or TUTs). Some PAPs/TUTs have more relaxed nucleotide specificity and carry out both uridylation and adenylation. Humans have seven noncanonical PAPs/TUTs with distinct substrate specificity and subcellular localization.

Uridylation of mRNA was initially noticed at the 3′ ends of miRNA-directed cleavage products in *Arabidopsis* and mammalian cells (Shen and Goodman, 2004). U-tails were also detected on human replication-dependent histone mRNAs that lack a poly(A) tail (Mullen and Marzluff, 2008). Histone mRNAs are uridylated and degraded at the end of S phase or upon inhibition of DNA replication (Mullen and Marzluff, 2008). TUT4 (ZCCHC11) was reported to catalyze histone mRNA uridylation (Schmidt et al., 2011; Su et al., 2013), although two other TUTs (TUT1/MTPAP/PAPD1 and TUT3/PAPD5/TRF4-2) were proposed in an earlier study (Mullen and Marzluff, 2008). Uridylation induces rapid decay of histone mRNA through both the 5′–3′ degradation by XRN1, DCP2, and LSM1 and the 3′–5′ degradation by exosome and ERI1 (3′hExo) (Hoefig et al., 2013; Mullen and Marzluff, 2008; Slevin et al., 2014).

Interestingly, uridylation occurs not only on poly(A)-lacking mRNAs but also on poly(A)$^+$ mRNAs, as shown first with the actin (*act1*) mRNA in fission yeast *Schizosaccharomyces pombe* (Rissland et al., 2007). When six mRNAs were examined by circularized rapid amplification of cDNA ends (cRACE) technique, all of them were found to bear short U-tails (usually one or two uridines) at the end of poly(A) tails albeit at varying frequencies, indicating that mRNA uridylation may be widespread in fission yeast (Rissland and Norbury, 2009). The stability of the *urg1* mRNA increased in a mutant lacking Cid1 which is one of the TUTs in fission yeast (Rissland et al., 2007; Rissland and Norbury, 2009). The uridylation frequency was enhanced in mutants defective of deadenylase and decapping enzyme (*ccr4*Δ and *dcp1-ts*). Based on these results, it was proposed that uridylation and deadenylation may act redundantly to induce decapping. A more recent study showed that *Arabidopsis* mRNAs are also subject to uridylation (Sement et al., 2013). Short uridyl residues (1–2 uridines) were detected on deadenylated, decapped mRNAs. The Cid1 homolog URT1 is required for uridylation. But, curiously, *URT1* mutation did not have a major impact on mRNA turnover and instead inhibited trimming of mRNA from the 3′ end (Sement et al., 2013), implying that uridylation may be necessary to establish the directionality (5′–3′) rather than to control the rate of mRNA decay. Therefore, although these

observations are intriguing, it was unclear if uridylation has a conserved function across species and whether animal poly(A)$^+$ mRNAs are also uridylated. In addition, because previous studies examined a few individual mRNAs by RACE and small-scale cloning, it remained to be tested whether or not uridylation occurs globally and if the observed changes in uridylation and poly(A) length are statistically significant.

To investigate tail structures at the genomic scale, we recently developed a method called TAIL-seq that deep-sequences the 3′ most fragments of RNAs (Chang et al., 2014b). The TAIL-seq protocol begins with removal of abundant noncoding RNAs such as rRNA, tRNA, small nuclear RNA (snRNA), and small nucleolar RNA (snoRNA) by affinity-based depletion and size fractionation. To avoid any bias against unconventional tails, TAIL-seq does not use splint ligation or oligo-d(T) enrichment. The resulting RNA sample enriched with mRNA is subsequently ligated to the 3′ adaptor that contains biotin residues. Following partial fragmentation, the 3′ most fragments are purified using streptavidin beads and ligated to the 5′ adaptor. Paired-end sequencing of the cDNA library yields 51 nt from the 5′ terminus of the fragment (to identify the transcript) and 231 nt from the 3′ terminus (to examine the tail sequences).

TAIL-seq provided us with a unique opportunity to investigate poly(A) tail length and additional 3′ modifications simultaneously at the genomic scale. Surprisingly, we found that the vast majority of mRNAs are subject to uridylation in mammals. Over 85% of mRNAs are terminally uridylated at a frequency of higher than 1% in both NIH 3T3 and HeLa cells (Chang et al., 2014b). Interestingly, U-tails are found mainly on mRNAs with short A-tails (less than ~25 nt), indicating that uridylation may occur following deadenylation. We further detected a negative correlation between uridylation frequency and mRNA half-life, suggesting a role of uridylation in general mRNA decay.

Current model for eukaryotic mRNA decay pathway is mainly based on the pioneering genetic and biochemical studies in *Saccharomyces cerevisiae* (Garneau et al., 2007; Houseley and Tollervey, 2009; Norbury, 2013; Parker and Song, 2004). Decay is generally initiated by deadenylation that is mediated by multiple deadenylases such as the Pan2-Pan3 complex and the Ccr4-Not complex. Subsequently, deadenylated mRNAs are subject to either of two major decay pathways. In the 5′–3′ decay pathway, the Lsm1–7 complex binds to the 3′ end of deadenylated mRNA and recruits the decapping complex (Dcp1/2) that removes 5′ cap structure. Subsequently, 5′ monophosphate-dependent exoribonuclease, Xrn1, digests mRNA processively. From the opposite orientation, a multisubunit exosome complex degrades deadenylated mRNAs from the 3′ end. This model seems to apply generally to most, if not all, eukaryotic species. However, *S. cerevisiae* is unusual among eukaryotes in that it does not have any known TUT homolog with uridylation activity and that mRNAs in *S. cerevisiae* do not carry terminal U-tails (Norbury, 2013). Thus, the current model for mRNA decay, particularly in mammals, may need to be revised to incorporate the recent findings of pervasive uridylation (Lee et al., 2014).

In this study, we aimed to identify enzyme(s) that catalyze mRNA uridylation in mammals and understand the significance of uridylation in the mRNA decay pathway. We discover TUT4 and TUT7 as uridylyl transferases for poly(A)$^+$ mRNAs in humans and delineate in detail the action mechanism and molecular function of uridylation in the mRNA decay pathway. Based on these results, we propose a revised model for general mRNA decay in mammals.

RESULT

TUT4 and TUT7 Catalyze mRNA Uridylation

In order to identify enzyme(s) responsible for mRNA uridylation, we took a candidate approach by depleting seven human TUTases (Figure S1A available online). Because TUT2 (also known as GLD2 and PAPD4), TUT4 (ZCCHC11), and TUT7 (ZCCHC6) act redundantly in mono-uridylation of precursor of let-7 (pre-let-7) (Heo et al., 2012), we knocked down TUTases in two subgroups (TUT1/3/5/6 and TUT2/4/7) by transfecting siRNA mixtures into HeLa cells (Figure S1B) and carried out TAIL-seq (Figure 1A). Overall frequency of uridylation was quantified by dividing the read number of terminally uridylated mRNAs by that of total mRNAs. Because short A-tails are preferentially uridylated (Chang et al., 2014b), uridylation frequency in short A-tail range (5–25 nt) is shown in Figure 1. Interestingly, when TUT2/4/7 were depleted, terminal uridylation was significantly reduced while RNAi of TUT1/3/5/6 did not affect uridylation.

To narrow down on individual TUTases, we generated knockout HeLa cell lines using TALENs (transcription activator-like effector nucleases) against the genes coding TUT2, TUT4, or TUT7 proteins (Figure S1C). We observed a modest decrease of uridylation in both *TUT4* and *TUT7* knockout cells, but not in *TUT2* knockout cells (Figure 1B). Repeated attempts to generate double knockout of *TUT4* and *TUT7* by utilizing the TALEN and CRISPR/Cas9 (clustered regularly interspaced short palindromic repeats/CRISPR-associated protein 9) systems have failed (Figure S1D). Although genomic deletion was effectively introduced by the nucleases, mutant clones disappeared during clonal selection processes (Figure S1D), which indicates that the combined activity of TUT4 and TUT7 is essential for cell viability.

Of note, previous studies have shown that TUT4 and TUT7 are highly similar in their domain organization and activity in pre-miRNA uridylation (Heo et al., 2012; Liu et al., 2014; Thornton et al., 2012). Thus, TUT4 and TUT7 (TUT4/7) may act redundantly in mRNA uridylation as well as in pre-miRNA uridylation. To confirm this notion, we carried out simultaneous transient RNAi against TUT4/7 by transfecting siRNAs (Figures 1C and S1E). The TUT4/7 knockdown cells looked largely normal and proliferated at a modestly reduced rate with a slight increase of apoptosis after 4 days of siRNA treatment (Figures S1F and S1G). Under this condition, uridylation of mRNA was significantly reduced when both TUT4 and TUT7 are depleted (Figure 1C). Oligo-uridylation ($\geq$2 U) was more sensitive to TUT4/7 knockdown than mono-uridylation was (3.71-fold and 1.36-fold decrease, respectively), suggesting that a relatively high level of TUT4/7 may be required to generate oligo-U-tails on mRNA.

Gene-level analyses revealed that the majority of mRNA species (638 out of 746 genes, 85.5%) are decreased in uridylation following TUT4/7 knockdown ($p = 7.69 \times 10^{-100}$, one-tailed Mann-Whitney U test) (Figure 1D; Table S1). This result strongly indicates that TUT4/7 uridylate most, if not all, mRNAs. Figure 1E presents 21 most abundant mRNAs as examples, the majority of

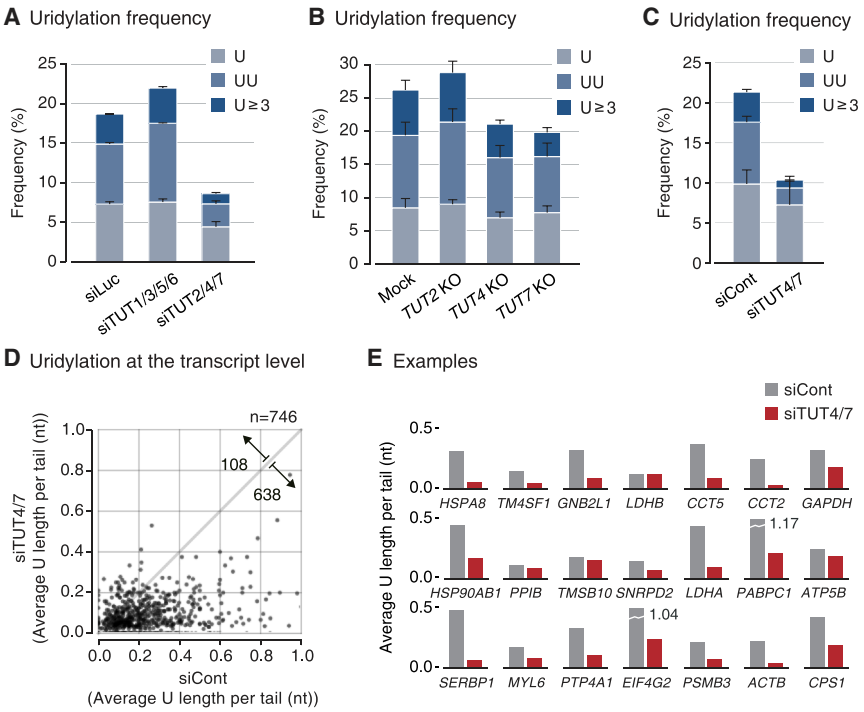

Figure 1. TUT4 and TUT7 Are Required for mRNA Uridylation in Human Cells

(A) Uridylation frequency measured by small-scale TAIL-seq (with Illumina MiSeq) following RNAi of the indicated genes. Frequency (y axis) is the fraction of uridylated reads among the total number of mRNA reads with short poly(A) tail (5–25 nt). Light blue refers to mono-uridylation (U), blue indicates di-uridylation (UU), and dark blue represents ≥ 3 uridines (U ≥ 3). Uridylation frequency significantly decreased in siTUT2/4/7 ($p = 0.0378$ for U; 0.0388 for UU; 0.0201 for U ≥ 3 by one-tailed t test). Error bar represents SEM from two biologically independent replicates (n = 2).

(B) Uridylation frequency of mRNAs with short poly(A) tails (5–25 nt) measured by small-scale TAIL-seq in knockout HeLa cell lines. Uridylation frequency was reduced modestly in *TUT4* and *TUT7* knockout cells ($p = 0.109$ for U, 0.0273 for UU, 0.142 for U ≥ 3 of *TUT4* KO; $p = 0.150$ for U, 0.00685 for UU, 0.0713 for U ≥ 3 of *TUT7* KO by one-tailed t test). Error bar represents SEM from two replicates (n = 2).

(C) Uridylation frequency of mRNAs with short poly(A) tails (5–25 nt) measured by TAIL-seq following simultaneous TUT4 and TUT7 knockdown (siTUT4/7). Uridylation was reduced when both TUT4 and TUT7 were depleted ($p = 0.0941$ for U, 0.00922 for UU, 0.0105 for U ≥ 3; one-tailed t test). Error bar represents SEM from three biological replicates (n = 3).

(D) Changes in uridylation of individual mRNA species upon TUT4/7 knockdown. "Average U length per tail" (y axis) is the sum of the number of all uridines on short A-tails (5–25 nt) divided by the total number of reads with short A-tails. Note that unlike "uridylation frequency," average U length per tail weighs every uridine in oligo-U-tails. Each dot represents a transcript with ≥ 15 reads in both samples. Uridylation was significantly decreased following TUT4/7 knockdown ($p = 7.69 \times 10^{-100}$, one-tailed Mann-Whitney U test). The full list is shown in Table S1.

(E) Examples of gene-level uridylation changes. Twenty-one most abundant mRNAs (not including ribosomal protein mRNAs and histone mRNAs) are shown in the order of mRNA abundance.

See also Figure S1.

which are reduced in uridylation upon TUT4/7 knockdown. Two biological replicate experiments showed a comparable decrease of uridylation (Figure S1H).

Histone mRNAs that lack poly(A) tails are also uridylated and their uridylation is dependent modestly on TUT4/7, but not on TUT1/2/3/5/6 (data not shown). However, poly(A)$^-$ histone mRNAs were excluded from our current data analyses because we used nonsynchronous cell population for our experiments, and it is known that uridylation of histone mRNA occurs specifically at the end of S phase (Mullen and Marzluff, 2008; Schmidt et al., 2011; Su et al., 2013). It would be more appropriate to investigate histone mRNAs using synchronous cells in future studies.

TUT4/7 Selectively Oligo-Uridylate mRNAs with Short A-Tails In Vivo and In Vitro

It is intriguing that uridylation occurs preferentially on shortened A-tails in plants and animals (Chang et al., 2014b; Sement et al., 2013). Figure 2A shows the distribution of U-tails over different lengths of A-tails in HeLa cells. The frequency of uridylation on the transcripts with a short A-tails (5–25 nt) is higher than that on the rest (A-tails of >25 nt), especially when only oligo-U (≥2 U) is counted. Note that mRNAs with A-tails of shorter than 5 nt were excluded from this analysis as it is sometimes difficult to distinguish them from genomic A-rich sequences in 3′ UTR. When TUT4/7 were depleted, uridylation on short A-tails was selectively reduced (especially for oligo-U), indicating that TUT4/7 are responsible for the specific uridylation of short A-tails (Figure 2A).

To understand the mechanism underlying such strong association with A-tail length, we performed in vitro uridylation assays using immunopurified full-length TUTases (Figures 2B and S2A–S2C). Substrate RNAs were chemically synthesized to contain heterogenous sequences (the last 20 nt from the *SHOC2* 3′ UTR) linked to A-tails of various lengths (0, 10, 25, and 50 nt) at the 3′ end (Figure 2B). We also used a "swapped" control (A25R) that has a 25 nt A segment at the 5′ side of the *SHOC2* 3′ UTR such that the RNA is identical to SHOC2-A25 (A25) in the overall length and base composition, but lacks an A-tail at the 3′ end (Figure 2B).

Interestingly, RNAs with no tail (A0) or a short A-tail (A10) were oligo-uridylated efficiently by TUT4 under the condition where pre-let-7a-1 is mono-uridylated weakly (Figure 2B). A25 and A50 were less efficiently uridylated than A0 and A10 were. The A25R RNA was a much better substrate than the A25 was, indicating that it is the 3′ A-tail length (not the overall RNA length) that is measured by TUT4 (Figure 2B). Comparable results were obtained with full-length TUT7 protein (Figures S2A and S2B), again

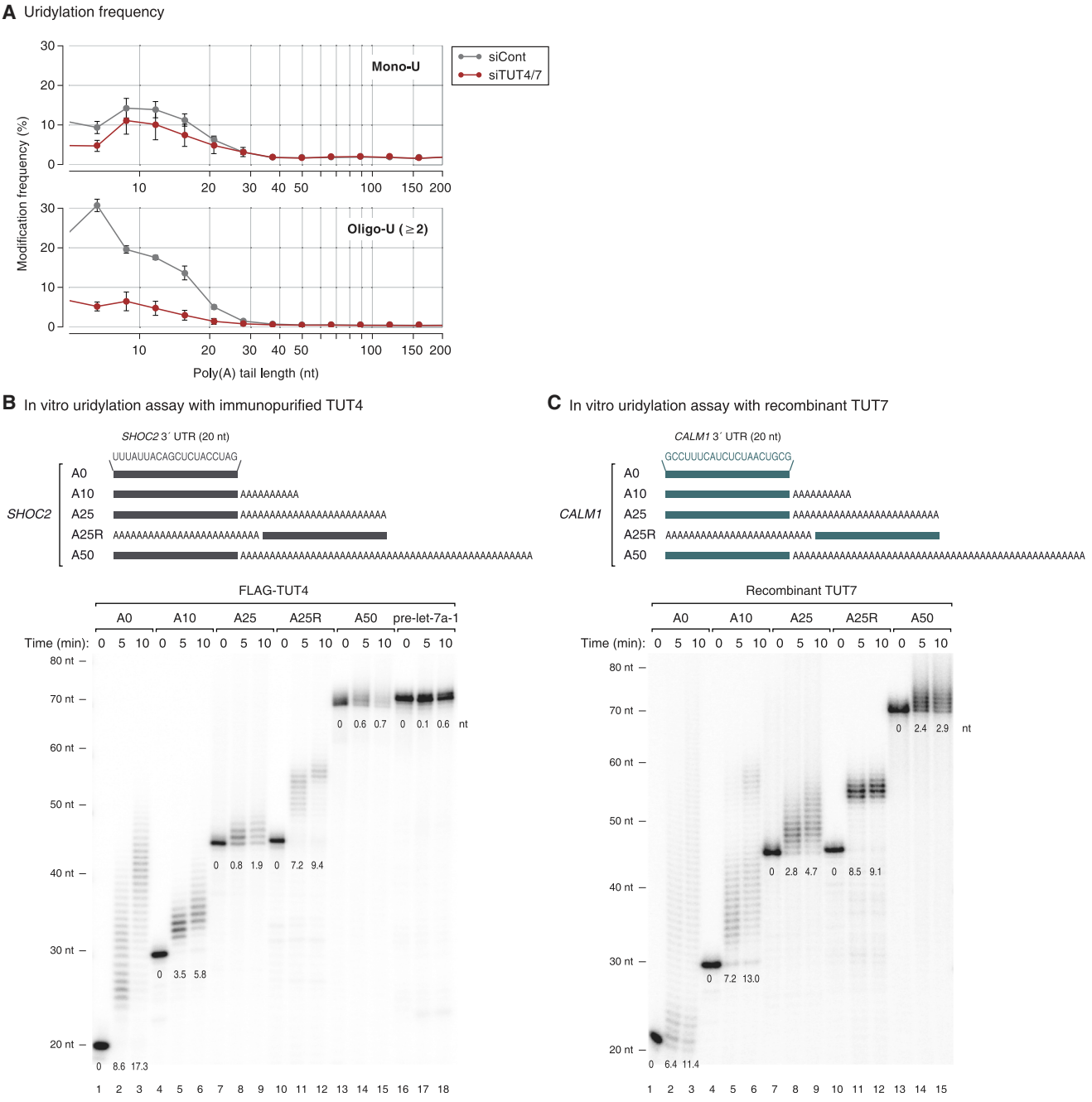

Figure 2. Short A-Tails Are Selectively Uridylated by TUT4 and TUT7

(A) Distribution of mono-uridylation (top) and oligo-uridylation (bottom) according to the length of poly(A) tails. Poly(A) tail lengths from 5 nt to 231 nt are pooled into equal-width bins in the logarithmic scale (base 2) (x axis). The left edges (inclusive) of bins are 5, 7, 9, 12, 15, 21, 28, 38, 50, 67, 89, 119, 159, and 212 nt. Uridylation frequency (y axis) indicates the percentage of uridylated reads within each poly(A) tail size range. Error bar represents SEM (n = 3).

(B) Top: illustration of chemically synthesized RNA substrates. Grey bars represent the last 20 nt of *SHOC2* 3′ UTR and "A" indicates an adenosine. Bottom: in vitro uridylation assay using immunopurified FLAG-TUT4. RNA (0.45 nM) was used in each reaction. The products were resolved on 6% polyacrylamide sequencing gel containing 7 M urea. The average length of uridylation is shown below each band. See Extended Experimental Procedures for quantification method.

(C) Top: illustration of chemically synthesized RNA substrates. Green bars represent the last 20 nt of *CALM1* 3′ UTR and "A" indicates an adenosine. Bottom: in vitro uridylation assay using recombinant TUT7 C-terminal fragment (951–1,495 aa) purified from *E. coli*. RNA (0.45 nM) and 14 nM of recombinant TUT7 were used in each reaction. Extension products were resolved on 6% polyacrylamide sequencing gel containing 7 M urea. The average length of uridylation was quantified as in (B).

See also Figure S2.

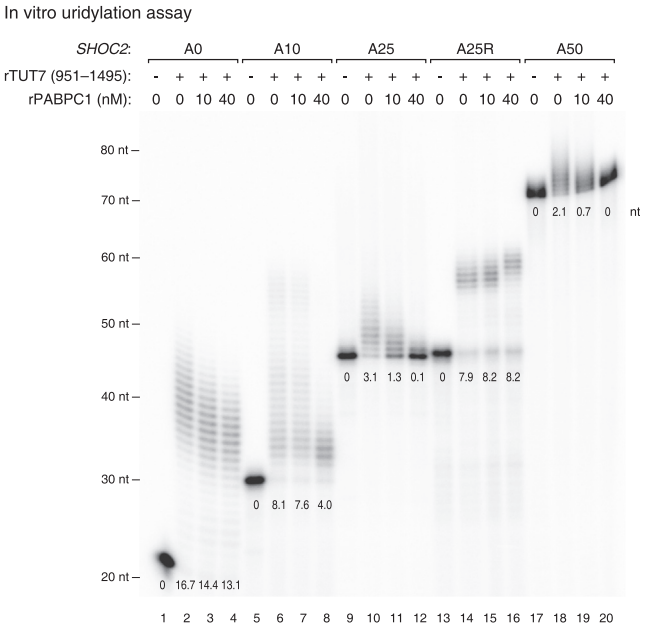

Figure 3. PABP Inhibits Uridylation of Polyadenylated mRNA

In vitro uridylation assay by using recombinant TUT7 (951–1,495 aa) with a varying concentration of recombinant PABPC1 (0, 10, or 40 nM). 0.45 nM of RNA and 160 nM of recombinant TUT7 (rTUT7) were used in the reaction. Extension products were resolved on 6% polyacrylamide sequencing gel containing 7 M urea. The average length of uridylation was quantified as described in Extended Experimental Procedures and shown below each band. See also Figure S3.

demonstrating that these two related enzymes are functional paralogs. The U-tail length in Figures S2A and S2B was overall shorter than those in Figure 2B because the amount of immunoprecipitated TUT7 was smaller than that of TUT4 in Figure 2B (data not shown).

We also prepared recombinant TUT7 protein (951–1,495 aa) from *Escherichia coli* and used the fragment for in vitro uridylation assay (Figure S2C). Apart from the *SHOC2* RNAs (Figure S2D), we synthesized and tested another series of RNAs based on the *CALM1* 3′ UTR sequences (Figure 2C). The purified protein fragment was fully capable of carrying out uridylation in an A-tail length-dependent manner with both RNAs (Figures 2C and S2D, see below). Thus, the C-terminal half of TUT7 is sufficient to recognize and uridylate single-stranded RNAs with a short A-tails (less than ~25 nt), in a 3′ UTR sequence-independent manner. These results suggest that TUT4/7 possess an intrinsic ability to measure the 3′ terminal A length and avoid uridylation of long A-tails.

PABP Suppresses Uridylation of Poly(A)$^+$ mRNA

As poly(A)$^+$ mRNAs are associated with poly(A) binding protein (PABP) in cells, we asked if PABP has an influence on mRNA uridylation. It was previously shown that PABP preferentially interacts with poly(A) or A-rich sequences (Eliseeva et al., 2013). The binding affinity increases as the A stretch gets longer (Eliseeva et al., 2013; Khanam et al., 2006; Kühn and Pieler, 1996; Sachs et al., 1987). Full-length PABP occupies an ~25 nt A-tail as determined by nuclease digestion assay (Baer and Kornberg, 1983; Eliseeva et al., 2013). In order to test an effect of PABP on uridylation, we carried out in vitro uridylation assays in the presence of recombinant PABPC1 (Figure 3). When PABPC1 was added to RNA, uridylation of RNAs with long poly(A) tail (A25 and A50) was suppressed even at a low concentration of PABPC1 (10 nM) while those with no or short A-tail (A0, A10, and A25R) remained largely unaffected (Figure 3). This result suggests that PABPC1 binds preferentially to long poly(A) tails and protects them from TUT4/7 and thereby enhances the selectivity of uridylation according to poly(A) tail length.

Taken together, our results suggest that the strict dependence on the A-tail length observed in vivo may be determined by the combination of two factors: (1) the intrinsic ability of TUT4/7 to measure poly(A) stretch (Figure 2), and (2) the protective activity of PABP (Figure 3).

As deadenylation is thought to occur mainly in the cytoplasm, we examined the localization of TUT4/7 by western blotting. The TUT4 and TUT7 proteins are mainly localized in the cytoplasm (Figure S3). Thus, TUT4/7 may function mainly in the metabolism of cytoplasmic, deadenylated mRNAs.

Uridylation Facilitates Global mRNA Decay

To understand the functional consequences of uridylation, we measured mRNA half-life in HeLa cells with or without TUT4/7 knockdown (Figure 4A). mRNA levels were determined by RNA-seq at 0, 1, 2, and 4 hr after actinomycin D treatment that blocks transcription. To avoid any bias from tail length variation, we omitted the oligo-dT enrichment step and instead used Ribo-Zero to remove abundant rRNAs prior to cDNA library construction. We could measure turnover rates of 1,829 mRNAs. In TUT4/7-depleted cells, the majority of mRNAs (1,426 out of 1,829 [78.0%]) showed increase stability (Figure 4A, left panel; Table S2). Half-lives were increased by ~30% on average, and median half-life was extended from 9.45 hr to 11.2 hr (Figure 4A, right panel).

Of note, although TUT4/7 contribute to let-7 biogenesis, double knockdown of TUT4/7 (without simultaneous knockdown of TUT2) did not substantially affect the let-7 level (Heo et al., 2012). In fact, our transcriptome analyses show that mRNAs are globally upregulated, indicating that the changes in mRNA half-life observed in this study cannot be attributed to specific regulation of let-7 biogenesis.

For validation of the impact of TUT4/7 depletion on mRNA stability, five mRNAs (*SHOC2*, *TRIM24*, *RB1CC1*, *MET*, and *XRN1*) were measured by quantitative RT-PCR after actinomycin D treatment (Figure 4B). None of these mRNAs contains a let-7 binding site with seed match in their 3′ UTR, yet all of them showed increased stability when TUT4/7 were depleted. Therefore, our results demonstrate that TUT4/7 play an important role in bulk mRNA degradation in a let-7 independent manner.

Next, to examine the effect of overexpressed TUTase on mRNA expression, we carried out tethering experiments in HeLa cells (Figure 4C, left panel). A related experiment was reported recently in *Xenopus* oocytes: when *Xenopus* TUT7 homolog was tethered to the 3′ UTR of luciferase reporter mRNA, luciferase activity was reduced without significant changes in mRNA, implicating translational repression (Lapointe and

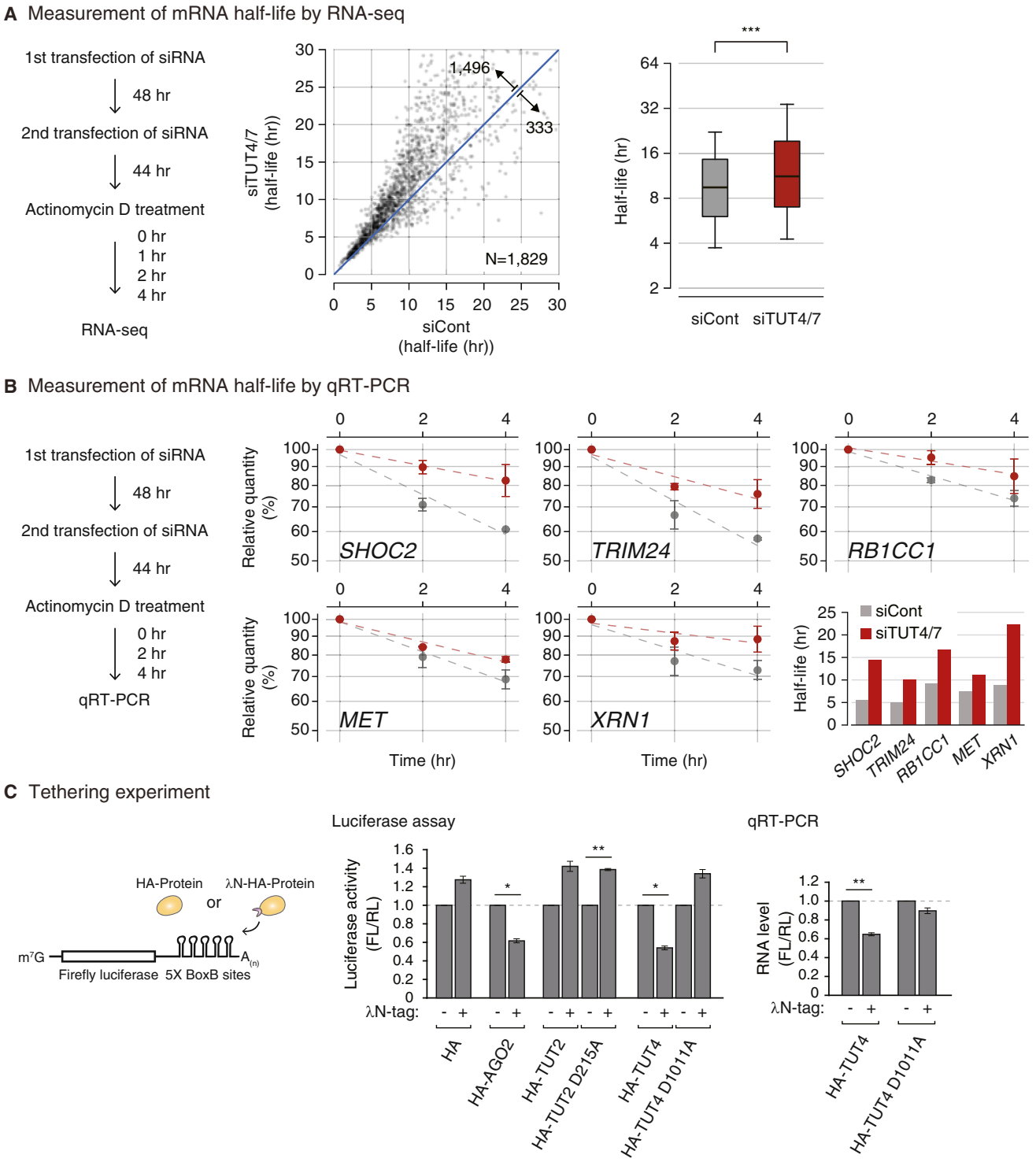

Figure 4. Uridylation Promotes mRNA Degradation

(A) Transcriptome-wide change of mRNA half-life determined by RNA-seq. Left: experimental scheme. HeLa cells were transfected twice and harvested at 0, 1, 2, and 4 hr following actinomycin D treatment. Center: changes of average mRNA half-life upon TUT4/7 knockdown from two biological replicates. The range of display is limited to between 0 and 30 hr for the better visual recognition (232 out of 1,829 mRNAs are outside of the view). The full list is available in Table S2. Right: distribution of mRNA half-lives in control or TUT4/7 knockdown cells. A box represents the first and third quartiles and an internal bar indicates median. Whiskers span between the ninth and the 91st percentiles. Half-lives of mRNAs are significantly extended by TUT4/7 knockdown (***$p = 4.06 \times 10^{-155}$, one-tailed paired Mann-Whitney U test). See Extended Experimental Procedures for the detailed description of procedure.

(legend continued on next page)

Wickens, 2013). However, because mRNA decay activity is generally suppressed in oocytes (Barckmann and Simonelig, 2013), it was unclear if the observation from frog oocytes can be generalized. For tethering experiments, we generated constructs that express proteins tagged with the λN peptide that interacts with its specific binding sites (BoxB sites) in the 3′ UTR of luciferase mRNA (Figures 4C and S4). Expression of λN protein modestly increased luciferase expression nonspecifically for an unknown reason (Figure 4C, middle panel). Nevertheless, tethering of AGO2 repressed luciferase reporter expression (Figure 4C), as previously shown (Pillai et al., 2004), indicating that this is a valid system to test the effect of RNA silencing factors. Neither the negative control TUT2 nor its mutant repressed luciferase reporter expression. But when wild-type TUT4 was tethered to the reporter mRNA, luciferase activity was decreased to ~60% while such reduction was not observed with the catalytically dead point mutant (D1011A) of TUT4 (Figure 4C, middle panel), indicating that TUT4 suppressed gene expression via uridylation. Quantitative RT-PCR further showed that tethering of TUT4 induced a reduction of mRNA (Figure 4C, right panel). Thus, our results collectively indicate that TUT4/7 function as suppressors of gene expression through mRNA destabilization.

Uridylation Is Involved in miRNA-Induced Gene Silencing

Our model predicts that if a gene-specific inducer of deadenylation is introduced into cells, uridylation of the given transcript will take place, which in turn will facilitate RNA decay. To test our model, we examined the effect of miRNA as an example, which is well established to induce specific deadenylation of its complementary targets (Ameres and Zamore, 2013; Djuranovic et al., 2011; Huntzinger and Izaurralde, 2011; Krol et al., 2010).

We first analyzed the TAIL-seq data from our previous experiment where miR-1 mimic was transfected into HeLa cells (Chang et al., 2014b). As expected, miR-1 targets undergo deadenylation and subsequent downregulation following miR-1 mimic transfection (Figure 5A, middle and lower panels, respectively). Importantly, we detected a specific increase of uridylation on miR-1 targets whereas the rest of genes stayed largely unaffected (Figure 5A, upper panel). This result is consistent with our model that deadenylation leads to uridylation.

We next measured turnover rates of miR-1 targets with or without TUT4/7 knockdown. The mRNAs tested (*PTMA*, *ADAR*, and *PGM2*) are normally stable (half-lives >24 hr) in cells that do not contain miR-1 (Figure 5B, black line). When miR-1 was introduced, their half-lives were shortened to 6.5, 10.0, and 9.4 hr, respectively (Figure 5B, blue line). Upon TUT4/7 depletion, the miR-1 target mRNAs were stabilized (with extended half-lives of 14.0, 36.1, and 18.1 hr, respectively) (Figure 5B, red line). Therefore, TUT4/7 are necessary for the facilitated decay of miRNA targets. We propose that other factors that cause deadenylation may also induce uridylation and decay, as shown here with an example of miR-1.

mRNA Decay Factors Remove Uridylated mRNAs

To understand downstream events of uridylation, we disrupted 5′–3′ or 3′–5′ exonucleolytic decay factors and examined the mRNA terminome (Figure S5A). The popsicle-shaped bars in Figure 6 display the relative quantity of reads with a U-tail (thick stem) or without a U-tail (thin stem). As U-tail frequencies vary depending on poly(A) tail length, different A-tail ranges are shown separately along the horizontal axis. For more information, the overall uridylation frequency and poly(A) length distribution are presented in Figures S5B and S5C, respectively.

In order to inhibit 5′–3′ decay, we initially depleted a major 5′–3′ exoribonuclease XRN1. Interestingly, interference of XRN1 resulted in a strong accumulation of uridylated mRNAs with short A-tails (≤25 nt) (Figure 6A). Additionally, when we depleted LSM1 (a component of the LSM1-7 complex that is known to facilitate decapping) or overexpressed dominant-negative mutants of the decapping complex (DCP1 and DCP2) (Chang et al., 2014a), we detected an increase of uridylation among short A-tailed mRNAs (≤25 nt) (Figure 6B). Short A-tailed mRNAs increased in abundance (particularly, in the 5–15 nt range) when the 5′–3′ decay was suppressed. Note that the level of uridylated mRNA was upregulated substantially (U_1–U_{3+}), accounting for the overall increase of mRNA reads in this range, while mRNAs without a U-tail did not change significantly (U_0). This result is consistent with a model that deadenylated, uridylated mRNAs are normally degraded rapidly by the 5′–3′ decay factors while poly(A)$^+$ mRNAs without U-tails are relatively stable. The LSM1–7 complex is known to preferentially bind to RNAs with 3′ terminal uridyl residues (Chowdhury et al., 2007; Sharif and Conti, 2013; Song and Kiledjian, 2007; Zhou et al., 2014) and facilitate decapping through PATL1 (Pat1p in yeast) (Marnef and Standart, 2010; Wilusz and Wilusz, 2013). Thus, a short U-tail may first be recognized by the LSM1–7 complex which in turn facilitates decapping (by the DCP1/2 complex) and subsequent 5′–3′ degradation (by XRN1).

We also investigated the contribution of the 3′–5′ decay pathway by depleting 3′ exonucleolytic factors. When we knocked-down RRP41, a core subunit of human exosome, we detected a substantial accumulation of uridylated mRNAs with short A-tails (Figure 6C). Combinatorial knockdown of RRP41 and XRN1 resulted in a more pronounced increase of uridylation (Figure 6C). Therefore, both decay pathways (5′–3′ and 3′–5′) may act at the downstream of uridylation. We also tested a 3′–5′ exonuclease DIS3L2 which is related to DIS3 and DIS3L. While DIS3 and DIS3L function as components of exosome,

(B) Measurement of mRNA half-life by qRT-PCR. Left: the experimental scheme. Right: following 0, 2, and 4 hr of actinomycin D treatment, relative abundance (y axis) of five selected genes were measured. For normalization, *GAPDH* mRNA was used because it was highly stable (half-life > 24 hr, data not shown) and did not change noticeably by TUT4/7 depletion. Error bar represents SEM (n = 3). Half-lives are calculated by linear fitting of the log-transformed exponential decay function.

(C) Left: schematic representation of reporter assay system with the λN tethering. Center: reporter (firefly) luciferase activity was measured and normalized to Renilla luciferase activity (n = 3). Right: reporter mRNA levels were determined by qRT-PCR (n = 4). Error bars represent SEM. Luciferase activity or RNA level were significantly reduced when AGO2 or TUT4 were tethered (*$p < 0.01$, **$p < 0.001$; two-tailed t test).

See also Figure S4.

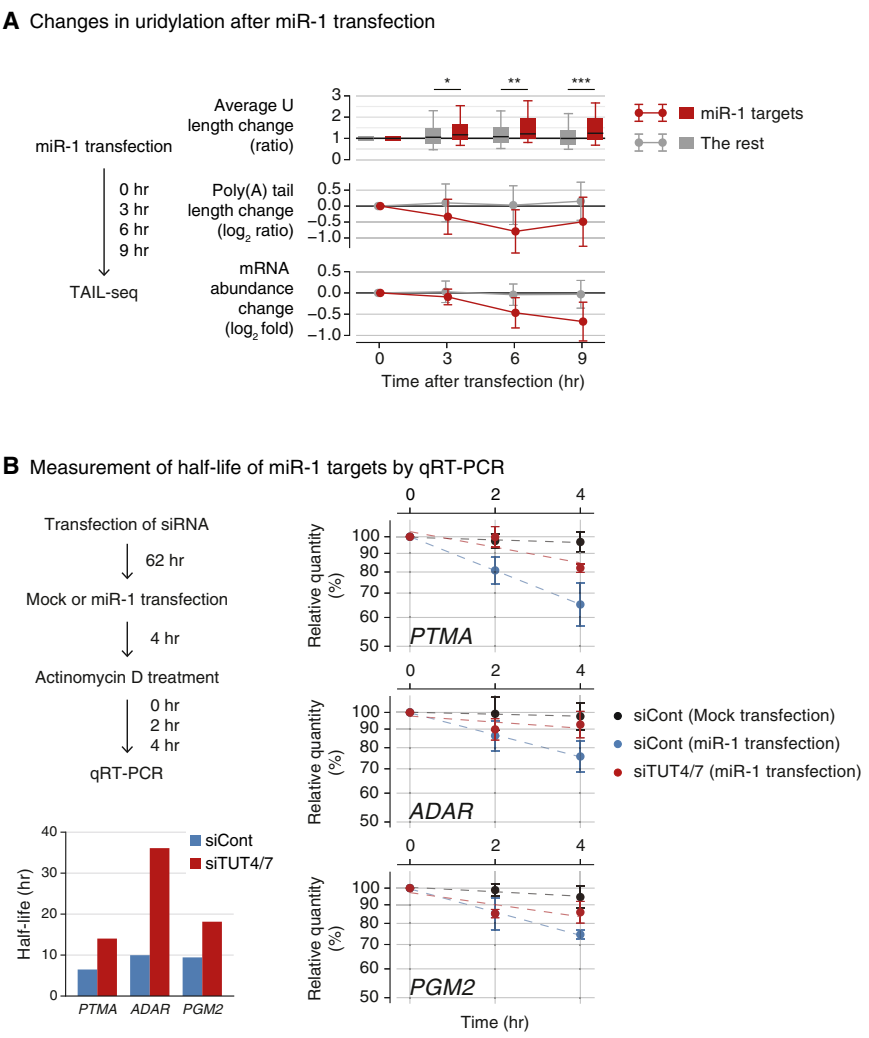

Figure 5. Uridylation Facilitates miRNA-Mediated mRNA Decay

(A) Changes in uridylation after miR-1 transfection. Left: experimental scheme. miR-1 was transfected into HeLa cells and the cells were harvested after the indicated time for TAIL-seq. Targets are the transcripts with ≥1 miR-1 3′ UTR site and down-regulated by ≥30% on 12 hr posttransfection of miR-1 (Guo et al., 2010). Right top: average U length change relative to 0 hr is shown in each time point. Average U length per tail is the number of uridines on short A-tails (5–25 nt) divided by the total number of reads with short A-tails. Box represents the interval between the first and third quartiles, and the internal bar indicates the median. Whiskers span between the ninth and 91st percentiles. Average U length of miR-1 target is significantly extended after miR-1 transfection (*p = 0.0152, **p = 0.00318, ***p = 5.79 × 10^{-4}; one-tailed Mann-Whitney U test). Right middle: poly(A) tail length change relative to 0 hr. The length change is represented by $\log_2$ odds ratio between long tails (>25 nt) and short tails (≤25 nt) in one among 3, 6, or 9 hr and 0 hr. A negative value (<0) indicates increase of the fraction of short tails compared to 0 hr. Error bars indicate SD among mRNAs. The portion of short poly(A) tails expanded more for miR-1 targets than the others (p = 1.80 × 10^{-6} for 3 hr, p = 8.47 × 10^{-13} for 6 hr, p = 1.48 × 10^{-11} for 9 hr; one-tailed Mann-Whitney U test). Right bottom: mRNA abundance ($poly(A)^+$ tag counts) change relative to 0 hr. Error bars indicate SD among mRNAs. Expression levels of miR-1 targets were decreased more than the rest transcripts (p = 2.09 × 10^{-4} for 3 hr, p = 2.65 × 10^{-14} for 6 hr, p = 5.46 × 10^{-18} for 9 hr; one-tailed Mann-Whitney U test).

(B) Measurement of half-life of miR-1 targets by qRT-PCR. Left: the experimental scheme. Following siRNA transfection for 62 hr, HeLa cells were transfected with miR-1 or mock transfected. After 4 hr, actinomycin D was treated and cells were harvested at 0, 1, 2, and 4 hr. Right: relative abundance (y axis) of miR-1 target mRNAs were measured. For the normalization, highly stable *GAPDH* mRNA was used because it did not change significantly by siTUT4/7 or miR-1 transfection. Error bar represents SEM (n = 3). Half-lives are determined by linear fitting of the log-transformed exponential decay function.

DIS3L2 is known to work independently from exosome (Lubas et al., 2013; Malecki et al., 2013). It was recently shown that DIS3L2 preferentially binds to long U-tails of pre-let-7 and is involved in turnover of pre-let-7 and some mRNAs in yeast and human (Chang et al., 2013; Faehnle et al., 2014; Lubas et al., 2013; Malecki et al., 2013; Ustianenko et al., 2013). Our TAIL-seq experiment shows that DIS3L2 depletion results in a modest accumulation of uridylated reads (Figure 6C). Thus, although we cannot rule out the possibility of indirect effects, our results suggest that multiple decay pathways may participate in the removal of uridylated mRNAs. Due to the technical limitation of knockdown experiment, it is currently unclear which pathway plays a dominant role.

Interestingly, mRNAs with an oligo-U-tail (U_2 and U_{3+}) responded more sensitively to the suppression of decay factors than those with a mono-U-tail (U_1), suggesting that oligo-uridylated mRNAs are more rapidly degraded than mono-uridylated mRNAs (Figures 6A–6C). Taken together, we propose that oligo-uridylated mRNAs are subject to degradation by multiple factors, and an oligo-U-tail may serve as a decay mark for nonfunctional, deadenylated mRNAs.

DISCUSSION

In conclusion, this study reveals an integral and general role of oligo-uridylation in mammalian mRNA decay (model shown in Figure 7). Upon deadenylation, mRNAs (with A-tails shorter than ~25 nt) lose PABP and instead gain a U-tail by the redundant action of TUT4 and TUT7. The oligo-U-tail triggers decay by serving as a mark that is recognized by downstream decay factors. Thus, TUT4/7 function as the "writers" of the decay mark. It will be interesting in the future to identify the "readers" of the oligo-U-tail and to ask if this modification can be reversed by "erasers." The LSM1–7 complex and DIS3L2 are likely candidates that recognize the oligo-U marks, but further investigations will be necessary to understand which factor(s) recognize the

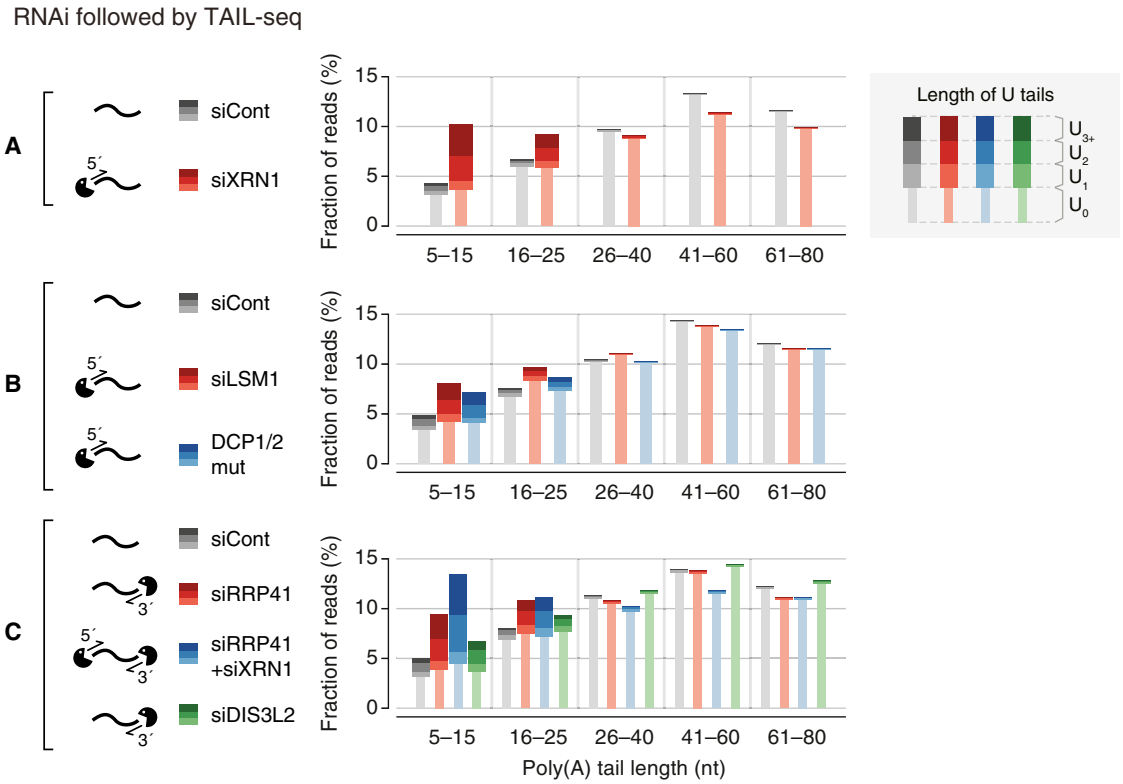

Figure 6. The 5′ and 3′ mRNA Decay Factors Degrade Uridylated mRNAs

(A–C) Changes of poly(A) tail and uridylation upon knockdown of decay factor(s) detected by small-scale TAIL-seq (with Illumina MiSeq). Fraction of mRNA reads out of the total poly(A)$^+$ mRNA reads is shown in each poly(A) tail size range. Narrow bars represent reads without U-tails (U_0) and wider bars indicate uridylated reads (U_1–U_{3+}). The "DCP1/2 mut" sample derived from cells coexpressed of dominant-negative mutants of DCP1 and DCP2 (DCP1a-GSSG and DCP2-E148Q, respectively).

See also Figure S5.

oligo-U-tails mainly, whether there is any additional factor(s) that binds to the oligo-U-tails, and what is the molecular basis of the specific recognition (Lee et al., 2014).

It is intriguing that TUT4/7 are capable of measuring poly(A) length (Figure 2). Poly(A) tail is unlikely to form a certain structure through base-pairing, so we do not yet understand how RNA with a poly(A) tail is discriminated by TUT4/7. It would be interesting to carry out structural studies on TUT4/7 and RNA with an A-tail of various length. Furthermore, we found that PABPC1 preferentially protects long poly(A) tails from uridylation (Figure 3). This specific inhibitory effect may come from the length-dependent binding of PABPC1 (Kühn and Pieler, 1996; Sachs et al., 1987). Thus, the combined action of TUT4/7 and PABP may selectively mark nonfunctional mRNAs while translationally active polyadenylated mRNAs are refractory to uridylation. Consequently, TUT4/7-mediated uridylation may provide the molecular basis for the tight control of mRNA stability according to poly(A) tail length.

We observed that oligo-uridylated mRNAs (with $\geq$2 uridines) are more sensitive than mono-uridylated mRNAs to the knockdown of TUT4/7 and decay factors. Moreover, oligo-U-tails are found in a narrow range of short A-tail length while mono-U-tails are more loosely distributed and found in polyadenylated mRNAs as well to some extent (Chang et al., 2014b). Thus, mono-uridylation appears to be less specific than oligo-uridylation and may be catalyzed in part by a TUT(s) other than TUT4/7. Furthermore, mono-U-tails may be too short to recruit decay factors effectively. Oligo-uridylated mRNAs are detected more frequently after depletion of decay factors, indicating that they are less stable than mono-uridylated mRNAs in control cells. Therefore, oligo-U-tails are likely to have a stronger effect in decay than mono-U-tails do. In fission yeast and plants, it is currently unclear if there is such a distinction between oligo-U-tails and mono-U-tails because only a small number of reads from cloning has been analyzed thus far.

Our transcriptome-wide analyses allowed us to propose a general model for the decay of poly(A)$^+$ mRNAs. In addition, given that poly(A)$^-$ histone mRNA was also proposed to be uridylated by TUT4 (Schmidt et al., 2011; Su et al., 2013), it is possible that both poly(A)$^+$ mRNAs and poly(A)$^-$ mRNAs are degraded by the same general principle involving uridylation although there may be some differences in details such as the choice of downstream decay factors. In fact, we detected uridylation on histone mRNAs and on trimmed decay intermediates lacking poly(A) tail and these U-tails were also dependent on TUT4/7 (data not shown).

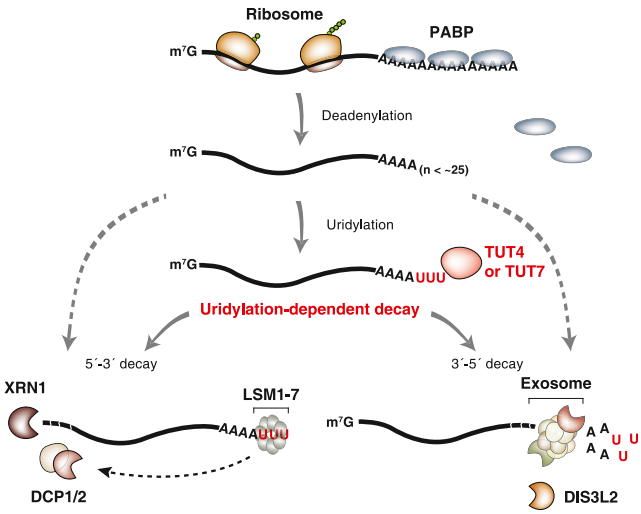

Figure 7. Model for Uridylation-Dependent mRNA Decay in Humans

mRNA decay is generally initiated by deadenylation. PABP proteins are dissociated from mRNA as poly(A) tail becomes shorter (less than ~25 nt). TUT4 and TUT7 act redundantly to uridylate mRNAs with a short A-tail. The U-tail is in turn recognized by the downstream decay factors (uridylation-dependent mRNA decay pathway). The LSM1–7 complex binds to the U-tail and facilitates decapping by the DCP1/2 complex. Decapped mRNAs are degraded by the 5′–3′ exonuclease XRN1. Alternatively, the U-tail is recognized by exosome or DIS3L2 that degrade mRNA exonucleolytically from the 3′ end. It is currently unclear if and what fraction of deadenylated mRNAs are degraded through uridylation-independent alternative pathways (indicated with gray dashed lines).

In addition, we found that miR-1 transfection results in an increased uridylation and facilitated decay of its targets (Figure 5). These results suggest that uridylation contributes to miRNA-mediated gene silencing by removing the body of deadenylated mRNAs. Uridylation may be involved in other decay and surveillance pathways in mammals, playing a general role. It is noted that we cannot currently assess if and to what extent uridylation-independent alternative pathway(s) contribute to bulk mRNA decay.

Tailing of mRNA is found in many eukaryotes, with some notable differences among the species. In filamentous fungus *Aspergillus nidulans*, mRNAs carry 3′ tails mixed with cytidine and uridine (Morozov et al., 2010). In a double deletion mutant of noncanonical PAPs, CutA and CutB, this "CUCU" modification was abrogated, and transcripts were stabilized, indicating that a CUCU tail also serves as a decay mark despite the difference in base composition (Morozov et al., 2010, 2012). In plants, although uridylation occurs similarly to mammals, mRNA half-life did not change in the *urt1* mutants, and the reason underlying the difference is currently unclear (Sement et al., 2013). Another variation among the species is that uridylation occurs selectively on deadenylated mRNAs in mammals and plants whereas uridylation appears to be independent of poly(A) tail length in *S. pombe* and *A. nidulans* (Morozov et al., 2010; Rissland and Norbury, 2009). Deadenylation may not be a prerequisite for uridylation in fungi as they possess shorter poly(A) tail (20–30 nt in median) than mammals (60–100 nt in median) and plants (50–60 nt in median) (Chang et al., 2014b; Morozov et al., 2010; Subtelny et al., 2014). Thus, further investigations are clearly necessary to delineate the commonalities and differences of uridylation in diverse systems.

Tailing-mediated decay is deeply conserved and found even in prokaryotes where mRNAs typically end with stem loop structure and are degraded in an adenylation-dependent manner (Belasco, 2010; Houseley et al., 2006). An oligo-A-tail serves as a single-stranded toehold for 3′ exonucleases that are otherwise hindered by the terminal stem loop. A related phenomenon was observed in budding yeast where noncanonical PAPs, Trf4 and Trf5, adenylate defective nuclear RNAs and facilitate their degradation by exosome (Houseley et al., 2006; Norbury, 2013). Our current work shows that mammalian cytoplasmic mRNAs use uridylation, instead of adenylation, to promote mRNA decay. Together with previous findings (Morozov et al., 2010; Mullen and Marzluff, 2008; Rissland and Norbury, 2009), our study establishes a fundamental and conserved role for tailing in the mRNA decay pathways.

EXPERIMENTAL PROCEDURES

Construction of TAIL-Seq Library

TAIL-seq was carried out as described previously (Chang et al., 2014b). Briefly, 25–50 μg of total RNA was extracted using TRIzol (Invitrogen), purified with RNeasy MinElute column (QIAGEN), and rRNA-depleted by using Ribo-Zero kit (Epicentre). The RNAs were ligated to the biotinylated 3′ adaptor and partially digested by RNase T1 (Ambion). The fragmented RNAs were precipitated with streptavidin beads, phosphorylated at the 5′ end, and gel purified (500–1,000 nt). The purified RNAs were ligated to the 5′ adaptor, reverse-transcribed, and amplified by PCR. The cDNA libraries were mixed with PhiX control library v3 (Illumina) and spike-in mixture and then sequenced by paired-end run (51 × 251 cycles) on Illumina MiSeq (small-scale TAIL-seq) or HiSeq 2500. Resulting data were processed as previously described (Chang et al., 2014b). See also Extended Experimental Procedures.

In Vitro Uridylation Assay

For immunoprecipitation of FLAG-TUTases, HEK293T cells grown on 10 cm dishes were collected 48 hr after transfection with FLAG-TUTase expression plasmids (full-length human TUT4 [1–1,640 aa] and human TUT7 [1–1,495 aa]). The cells were incubated in ice-cold Buffer D (200 mM KCl, 10 mM Tris-HCl [pH 8.0], 0.2 mM EDTA) for 20 min followed by sonication on ice and centrifugation twice for 15 min at 4°C. The supernatant was incubated with 5 μl of anti-FLAG antibody-conjugated agarose beads (anti-FLAG M2 affinity gel, Sigma) with constant rotation for 1 hr at 4°C. The beads were washed six times with Buffer D. Uridylation reaction was done in a total volume of 30 μl in 3.2 mM $MgCl_2$, 1 mM DTT, 0.67 U/μl RNase inhibitor (Promega, N2515), 0.25 mM UTP, 0.45 nM of 5′ end-labeled RNA, and 15 μl of immunopurified proteins on beads or 3X Flag-peptide (Sigma) eluted proteins in Buffer D. When uridylation assay was done with recombinant TUT7 (951–1,495 aa), 14 nM of protein was used. The reaction mixture was incubated at 37°C for up to 10 min. For uridylation assay in the presence of PABPC1, 10–40 nM of recombinant human PABPC1 (Origene, TP307354) was preincubated with RNA for 10 min and then uridylation was carried out by adding 160 nM of recombinant TUT7 (951–1,495 aa). Buffer D with final 300 mM KCl was used when uridylation assay was carried out in the presence of PABPC1. The RNA was purified from the reaction mixture by phenol extraction and run on 6% polyacrylamide sequencing gel with 7 M urea (20 × 40 cm, 0.4 mm thick) at constant 1,500 V for 2 hr. The gel was exposed to phosphor imaging plate (Fujifilm) and read by Typhoon FLA 7000 (GE Healthcare). The signal intensity profile was quantified using MultiGauge v3.0 (Fujifilm). In Figure S2D, 12.5% polyacrylamide gel was used. The *SHOC2* 3′ UTR and *CALM1* 3′ UTR were selected as RNA substrates as they do not contain homopolymeric adenosines at the 3′ end. RNAs were synthesized by ST Pharm.

The list of RNA oligos is shown in Table S3.

ACCESSION NUMBERS

The NCBI Gene Expression Omnibus (GEO) accession number for the sequenced reads reported in this paper is GSE59628.

SUPPLEMENTAL INFORMATION

Supplemental Information includes Extended Experimental Procedures, five figures, and three tables and can be found with this article online at http://dx.doi.org/10.1016/j.cell.2014.10.055.

AUTHOR CONTRIBUTIONS

J.L., M.H., H.C., and V.N.K. designed experiments. J.L., M.H., and S.C.K. performed biochemical and cell biological experiments. H.C. carried out computational analyses. D.K.S. and D.J.P. prepared recombinant proteins. J.L., M.H., H.C., and V.N.K. wrote the manuscript.

ACKNOWLEDGMENTS

We are grateful to members of our laboratory for discussion and technical help, especially Eunji Kim for help with plasmid cloning. We thank Dr. E. Izaurralde for insightful suggestions and the gifts of DCP1/2 mutant plasmids and Dr. G. Dreyfuss for the gift of anti-PABPC1 antibody. This work was supported by IBS-R008-D1 of Institute for Basic Science from the Ministry of Science, ICT and Future Planning of Korea (J.L., M.H., H.C., S.C.K., and V.N.K.) and the BK21 Research Fellowships from the Ministry of Education of Korea (J.L.).

Received: July 16, 2014
Revised: September 24, 2014
Accepted: October 20, 2014
Published: December 4, 2014

REFERENCES

Ameres, S.L., and Zamore, P.D. (2013). Diversifying microRNA sequence and function. Nat. Rev. Mol. Cell Biol. *14*, 475–488.

Aravind, L., and Koonin, E.V. (1999). DNA polymerase beta-like nucleotidyltransferase superfamily: identification of three new families, classification and evolutionary history. Nucleic Acids Res. *27*, 1609–1618.

Baer, B.W., and Kornberg, R.D. (1983). The protein responsible for the repeating structure of cytoplasmic poly(A)-ribonucleoprotein. J. Cell Biol. *96*, 717–721.

Barckmann, B., and Simonelig, M. (2013). Control of maternal mRNA stability in germ cells and early embryos. Biochim. Biophys. Acta *1829*, 714–724.

Belasco, J.G. (2010). All things must pass: contrasts and commonalities in eukaryotic and bacterial mRNA decay. Nat. Rev. Mol. Cell Biol. *11*, 467–478.

Chang, H.M., Triboulet, R., Thornton, J.E., and Gregory, R.I. (2013). A role for the Perlman syndrome exonuclease Dis3l2 in the Lin28-let-7 pathway. Nature *497*, 244–248.

Chang, C.T., Bercovich, N., Loh, B., Jonas, S., and Izaurralde, E. (2014a). The activation of the decapping enzyme DCP2 by DCP1 occurs on the EDC4 scaffold and involves a conserved loop in DCP1. Nucleic Acids Res. *42*, 5217–5233.

Chang, H., Lim, J., Ha, M., and Kim, V.N. (2014b). TAIL-seq: genome-wide determination of poly(A) tail length and 3′ end modifications. Mol. Cell *53*, 1044–1052.

Chowdhury, A., Mukhopadhyay, J., and Tharun, S. (2007). The decapping activator Lsm1p-7p-Pat1p complex has the intrinsic ability to distinguish between oligoadenylated and polyadenylated RNAs. RNA *13*, 998–1016.

Djuranovic, S., Nahvi, A., and Green, R. (2011). A parsimonious model for gene regulation by miRNAs. Science *331*, 550–553.

Dreyfus, M., and Régnier, P. (2002). The poly(A) tail of mRNAs: bodyguard in eukaryotes, scavenger in bacteria. Cell *111*, 611–613.

Eliseeva, I.A., Lyabin, D.N., and Ovchinnikov, L.P. (2013). Poly(A)-binding proteins: structure, domain organization, and activity regulation. Biochemistry Mosc. *78*, 1377–1391.

Faehnle, C.R., Walleshauser, J., and Joshua-Tor, L. (2014). Mechanism of Dis3l2 substrate recognition in the Lin28-let-7 pathway. Nature *514*, 252–256.

Garneau, N.L., Wilusz, J., and Wilusz, C.J. (2007). The highways and byways of mRNA decay. Nat. Rev. Mol. Cell Biol. *8*, 113–126.

Guo, H., Ingolia, N.T., Weissman, J.S., and Bartel, D.P. (2010). Mammalian microRNAs predominantly act to decrease target mRNA levels. Nature *466*, 835–840.

Heo, I., Ha, M., Lim, J., Yoon, M.J., Park, J.E., Kwon, S.C., Chang, H., and Kim, V.N. (2012). Mono-uridylation of pre-microRNA as a key step in the biogenesis of group II let-7 microRNAs. Cell *151*, 521–532.

Hoefig, K.P., Rath, N., Heinz, G.A., Wolf, C., Dameris, J., Schepers, A., Kremmer, E., Ansel, K.M., and Heissmeyer, V. (2013). Eri1 degrades the stem-loop of oligouridylated histone mRNAs to induce replication-dependent decay. Nat. Struct. Mol. Biol. *20*, 73–81.

Houseley, J., and Tollervey, D. (2009). The many pathways of RNA degradation. Cell *136*, 763–776.

Houseley, J., LaCava, J., and Tollervey, D. (2006). RNA-quality control by the exosome. Nat. Rev. Mol. Cell Biol. *7*, 529–539.

Huntzinger, E., and Izaurralde, E. (2011). Gene silencing by microRNAs: contributions of translational repression and mRNA decay. Nat. Rev. Genet. *12*, 99–110.

Khanam, T., Muddashetty, R.S., Kahvejian, A., Sonenberg, N., and Brosius, J. (2006). Poly(A)-binding protein binds to A-rich sequences via RNA-binding domains 1+2 and 3+4. RNA Biol. *3*, 170–177.

Krol, J., Loedige, I., and Filipowicz, W. (2010). The widespread regulation of microRNA biogenesis, function and decay. Nat. Rev. Genet. *11*, 597–610.

Kühn, U., and Pieler, T. (1996). Xenopus poly(A) binding protein: functional domains in RNA binding and protein-protein interaction. J. Mol. Biol. *256*, 20–30.

Lapointe, C.P., and Wickens, M. (2013). The nucleic acid-binding domain and translational repression activity of a Xenopus terminal uridylyl transferase. J. Biol. Chem. *288*, 20723–20733.

Lee, M., Kim, B., and Kim, V.N. (2014). Emerging roles of RNA modification: m(6)A and U-tail. Cell *158*, 980–987.

Liu, X., Zheng, Q., Vrettos, N., Maragkakis, M., Alexiou, P., Gregory, B.D., and Mourelatos, Z. (2014). A MicroRNA precursor surveillance system in quality control of MicroRNA synthesis. Mol. Cell *55*, 868–879.

Lubas, M., Damgaard, C.K., Tomecki, R., Cysewski, D., Jensen, T.H., and Dziembowski, A. (2013). Exonuclease hDIS3L2 specifies an exosome-independent 3′-5′ degradation pathway of human cytoplasmic mRNA. EMBO J. *32*, 1855–1868.

Malecki, M., Viegas, S.C., Carneiro, T., Golik, P., Dressaire, C., Ferreira, M.G., and Arraiano, C.M. (2013). The exoribonuclease Dis3L2 defines a novel eukaryotic RNA degradation pathway. EMBO J. *32*, 1842–1854.

Marnef, A., and Standart, N. (2010). Pat1 proteins: a life in translation, translation repression and mRNA decay. Biochem. Soc. Trans. *38*, 1602–1607.

Martin, G., and Keller, W. (2007). RNA-specific ribonucleotidyl transferases. RNA *13*, 1834–1849.

Morozov, I.Y., Jones, M.G., Razak, A.A., Rigden, D.J., and Caddick, M.X. (2010). CUCU modification of mRNA promotes decapping and transcript degradation in Aspergillus nidulans. Mol. Cell. Biol. *30*, 460–469.

Morozov, I.Y., Jones, M.G., Gould, P.D., Crome, V., Wilson, J.B., Hall, A.J., Rigden, D.J., and Caddick, M.X. (2012). mRNA 3′ tagging is induced by nonsense-mediated decay and promotes ribosome dissociation. Mol. Cell. Biol. *32*, 2585–2595.

Mullen, T.E., and Marzluff, W.F. (2008). Degradation of histone mRNA requires oligouridylation followed by decapping and simultaneous degradation of the mRNA both 5′ to 3′ and 3′ to 5′. Genes Dev. *22*, 50–65.

Norbury, C.J. (2013). Cytoplasmic RNA: a case of the tail wagging the dog. Nat. Rev. Mol. Cell Biol. *14*, 643–653.

Parker, R., and Song, H. (2004). The enzymes and control of eukaryotic mRNA turnover. Nat. Struct. Mol. Biol. *11*, 121–127.

Pillai, R.S., Artus, C.G., and Filipowicz, W. (2004). Tethering of human Ago proteins to mRNA mimics the miRNA-mediated repression of protein synthesis. RNA *10*, 1518–1525.

Rissland, O.S., and Norbury, C.J. (2009). Decapping is preceded by 3′ uridylation in a novel pathway of bulk mRNA turnover. Nat. Struct. Mol. Biol. *16*, 616–623.

Rissland, O.S., Mikulasova, A., and Norbury, C.J. (2007). Efficient RNA polyuridylation by noncanonical poly(A) polymerases. Mol. Cell. Biol. *27*, 3612–3624.

Sachs, A.B., Davis, R.W., and Kornberg, R.D. (1987). A single domain of yeast poly(A)-binding protein is necessary and sufficient for RNA binding and cell viability. Mol. Cell. Biol. *7*, 3268–3276.

Schmidt, M.J., West, S., and Norbury, C.J. (2011). The human cytoplasmic RNA terminal U-transferase ZCCHC11 targets histone mRNAs for degradation. RNA *17*, 39–44.

Sement, F.M., Ferrier, E., Zuber, H., Merret, R., Alioua, M., Deragon, J.M., Bousquet-Antonelli, C., Lange, H., and Gagliardi, D. (2013). Uridylation prevents 3′ trimming of oligoadenylated mRNAs. Nucleic Acids Res. *41*, 7115–7127.

Sharif, H., and Conti, E. (2013). Architecture of the Lsm1-7-Pat1 complex: a conserved assembly in eukaryotic mRNA turnover. Cell Reports *5*, 283–291.

Shen, B., and Goodman, H.M. (2004). Uridine addition after microRNA-directed cleavage. Science *306*, 997.

Slevin, M.K., Meaux, S., Welch, J.D., Bigler, R., Miliani de Marval, P.L., Su, W., Rhoads, R.E., Prins, J.F., and Marzluff, W.F. (2014). Deep sequencing shows multiple oligouridylations are required for 3′ to 5′ degradation of histone mRNAs on polyribosomes. Mol. Cell *53*, 1020–1030.

Song, M.G., and Kiledjian, M. (2007). 3′ Terminal oligo U-tract-mediated stimulation of decapping. RNA *13*, 2356–2365.

Su, W., Slepenkov, S.V., Slevin, M.K., Lyons, S.M., Ziemniak, M., Kowalska, J., Darzynkiewicz, E., Jemielity, J., Marzluff, W.F., and Rhoads, R.E. (2013). mRNAs containing the histone 3′ stem-loop are degraded primarily by decapping mediated by oligouridylation of the 3′ end. RNA *19*, 1–16.

Subtelny, A.O., Eichhorn, S.W., Chen, G.R., Sive, H., and Bartel, D.P. (2014). Poly(A)-tail profiling reveals an embryonic switch in translational control. Nature *508*, 66–71.

Thornton, J.E., Chang, H.M., Piskounova, E., and Gregory, R.I. (2012). Lin28-mediated control of let-7 microRNA expression by alternative TUTases Zcchc11 (TUT4) and Zcchc6 (TUT7). RNA *18*, 1875–1885.

Ustianenko, D., Hrossova, D., Potesil, D., Chalupnikova, K., Hrazdilova, K., Pachernik, J., Cetkovska, K., Uldrijan, S., Zdrahal, Z., and Vanacova, S. (2013). Mammalian DIS3L2 exoribonuclease targets the uridylated precursors of let-7 miRNAs. RNA *19*, 1632–1638.

Wilusz, C.J., and Wilusz, J. (2013). Lsm proteins and Hfq: Life at the 3′ end. RNA Biol. *10*, 592–601.

Zhou, L., Zhou, Y., Hang, J., Wan, R., Lu, G., Yan, C., and Shi, Y. (2014). Crystal structure and biochemical analysis of the heptameric Lsm1-7 complex. Cell Res. *24*, 497–500.

EXTENDED EXPERIMENTAL PROCEDURES

Cell Culture, Transfection, and Drug Treatment

HeLa and HEK293T cells were maintained in DMEM (Welgene) supplemented with 10% fetal bovine serum (Welgene). Knockout HeLa cell lines were generated by ToolGen Inc. by using TALENs targeting exons of *TUT2*, *TUT4*, and *TUT7*. For knockdown, HeLa cells were transfected twice with 40 nM of siRNAs using Lipofectamine 2000 (Invitrogen) for 4 days. A mixture of 2–4 different siRNAs was used to knockdown each gene. In combinatorial knockdown, we mixed siRNA pools to have a final concentration of 40 nM. We purchased siRNAs against *LSM1* and *DIS3L2* from ON-TARGETplus SMARTpool (Dharmacon). The sequence list of siRNAs is shown in Table S3. To block transcription, HeLa cells were treated with actinomycin D (Sigma, 4 μg/ml). To introduce miR-1, synthetic miR-1 mimic was transfected ~48 hr after siRNA transfection, and cells were collected every 2 hr. For plasmid transfection, HeLa cells were transfected by using Lipofectamine 2000 and HEK293T cells were transfected by the calcium-phosphate method for 2 days. Human DCP1a GSSG mutant (1–582 aa) and human DCP2 E148Q mutant (1–420 aa) plasmids are gifts from Dr. Elisa Izaurralde.

Determination of Nontemplated Terminal Nucleotidyl Addition

After the primary measurement of poly(A) length from the TAIL-seq pipeline (Chang et al., 2014b), the poly(A) lengths are refined using a paired-end alignment of reads 1 and 2 to the UCSC hg19 genome using GSNAP 2013-03-31 (Wu and Nacu, 2010) to exclude genome-encoded A repeats from the measurement. First, the poly(A) length from the signal processing are considered valid when read 2 is not aligned. For those that aligned to the genome, the pairs of reads (1 and 2) are excluded from statistics when nearest alignments between them are farther away than 500,000 bp in genome coordinates so as to remove ligation artifacts. For the remaining ones, the 3′-most two nucleotides from 'matched or mismatched' ('M' in CIGAR string) are re-examined if they match to the genome. If there is any mismatch in the pairs, the first mismatched nucleotide and subsequent nucleotides including clipped ('S' in CIGAR string) are regarded as nontemplated additions. Otherwise, the clipped sequences on the 3′-end of reads are considered as nontemplated additions.

For the calculation of uridylation frequency or average U length, we exclude very short poly(A) tails between 1 and 4 nucleotides because a substantial fraction of them are ambiguous whether or not they come from genomic sequences or nontemplated additions. We also exclude noncoding RNAs (mainly snoRNA precursors) and histone mRNAs due to their distinct nature of metabolism from the major portion of mRNAs. For shorter poly(A) tails ($\leq$10 nt), we sort them again to remove artifacts from unwanted RNA ligations between the 3′ end of an mRNA and the 5′ end of abundant small RNAs (such as 5S rRNA, 5.8S rRNA, let-7, and miR-21). They are considered as poly(A) tails only if 80% or more in the nontemplated addition is composed of adenosines after trimming all consecutive uridines from the 3′ end. The length of U tails are measured by counting perfectly consecutive appearances of uridines from the 3′ end within the nontemplated additions.

RNA-Seq and Calculation of RNA Half-Lives

Total RNA was extracted with TRIzol (Invitrogen), and the quality was checked by Agilent 2100 Bioanalyzer. rRNA was depleted from total RNA using Ribo-Zero (Epicentre). RNA-seq libraries were constructed by Macrogen Inc. using Illumina TruSeq RNA sample preparation kit v2. The reads were aligned to UCSC hg19 genome assembly using STAR (Dobin et al., 2013) with an option "––outFilterScoreMin 3" and splicing junction annotations generated from the NCBI RefSeq and the UCSC knownGene. The reduced RefSeq transcript set for nonoverlapping representation was prepared as previously described (Chang et al., 2014b). Reads mapped to each transcript were counted using BEDTools multicov (Quinlan and Hall, 2010) with default options. Read counts of the 3, 6, and 9 hr samples were scale-normalized against those of the 0 hr sample. A scaling factor was calculated using all mRNAs with $\geq$ 5,000 raw reads from the 0 hr sample so that the 98th percentile of fold changes between 0 hr and other time points become 1 (unchanged). All mRNAs sequenced by $\geq$ 300 scaled reads at any time point were used for further processing. The scaled read counts were used for linear fitting to the log-transformed solution $\log N(t) = -\lambda t + \log N_0$ of the exponential decay function $dN = -\lambda N$, where N is the amount of a specific mRNA, λ is the decay rate constant, t is time elapsed after the initial time point. To ensure reliability, mRNAs with significant fitting error (residual $\geq$ 10% of decay constant) were removed from the analysis. We discovered half-life values are often systematically biased by various scaling-related factors unlike the original decay constant (λ). To cancel out those errors, we shifted linearly the calculated decay constants to let the linear trend line (derived using least-squares regression) pass through the origin for decay constants from siControl and siTUT4/7 samples perpendicularly to the trend line. As this does not change the slope of trend lines for decay constants, this adjustment does not affect direct interpretations of the decay constants. Half-life of an mRNA was calculated using an equation

$$h = \frac{\log 2}{\lambda},$$

where h is the half-life. The full list of calculated half-life and decay constant values are accompanied in Table S2.

Analysis for Uridylation, Poly(A) Tail Length, and Abundance of miR-1 Targets

Among all transcripts having $\geq$ 1 "miR-1ab/206/613" target site in TargetScan human release 6.2 (http://www.targetscan.org/vert_61/ — "61" is not a typo), we chose experimentally validated targets whose expression is represented by $\geq$ 100 raw reads

in mock treatment and depressed by ≥ 30% in RPM-normalized reads in miR-1 treated sample in the experiment by Guo and colleagues (Guo et al., 2010). "The rest" in Figure 5A are the remaining mRNAs after selecting the experimentally validated targets of miR-1 among the detectable mRNAs (for detection threshold, see below).

For the average U length changes (top) in Figure 5A, we selected all mRNAs whose short poly(A)$^+$ tags (5–25 nt) are ≥ 15 (raw reads) in the 0 hr samples of both siControl- and siTUT4/7-treated sets. For the poly(A) tail length changes (middle) and mRNA abundance changes (bottom), we selected all mRNAs whose poly(A)$^+$ tags (≥5 nt) are more than a hundred reads in the 0 hr samples of both siControl- and siTUT4/7-treated sets. Odds between short and long tails were calculated with a pseudocount of 1 to both.

Quantification of In Vitro Uridylation Data

The signal intensity profiles (20 pixels/mm) were calculated from the whole blot phosphorimages using Fujifilm MultiGauge v3.0. For each lane, background signal is estimated using the arithmetic mean of the 25th and the 50th percentiles of the signal intensities. The signal intensities were subtracted by the estimated background level, then clipped to zero so that all intensities have zero or positive values. For the alignment of bands for size markers, the signals from a marker lane were transformed to the first and second derivatives using Savitzky-Golay filter (window = 31 pixels, order = 3). The marker positions were detected by searching points where the sign of first derivative turns from positive to negative, and the second derivative is smaller than −100. The detected positions of marker bands were verified by visual inspection. The function between physical position in the gel and RNA size was defined using cubic spline interpolation. The density of RNA amount in size space was calculated using the first order discrete differences of equal-width samples (0.1 nt) from cumulative density of the original intensity values. For the average length of extensions, the position having maximum signal intensity in the 0 min sample is used as a reference position. The average length of extension was derived from an equation,

$$\bar{x} = \frac{\sum_p (s_p - r) I_p}{\sum_p I_p},$$

where $\bar{x}$ is the average length of extension, p is a position in the gel (by 0.1 nt-wide intervals), s_p is the RNA size in nucleotides count for position p, r is the reference size of unextended RNA, and I_p is signal intensity for position p. We excluded signals from degraded products (shorter than the reference size by 3 nt) in the calculation of average extension. The average lengths of extension in Figures 2B, 2C, and 3A are shown as the difference between the average extension at 0 min and that at the other time points.

Plasmid Construction

The λN sequence was amplified from pAc5.1B-λN-HA (Addgene #21302) using 'CTTGACACGAAGCTTATGGACGCACAAACAC GAC' and 'GTTACTAGTGGATCCACCTTGAAAATACAAGTTTTCGGCATAGTCAGGCACGTCATAAGGATAAGCCATATGTGGAG GAGATCC' and subcloned into the pCK vector (a CMV promoter-driven vector) using EZ cloning kit (Enzynomics, EZ016S), to generate pCK-λN-HA-TEV. The coding sequences of AcGFP (from pLVX-EF1alpha-AcGFP-N1; Clontech, 631983), human AGO2 (1-859 aa), human TUT2 (1-484 aa), and human TUT4 (1-1,640 aa) were subcloned into pCK-λN-HA-TEV and pCK-HA-TEV (control). The 5XBoxB sequence was amplified from pAc5.1C-FLuc-Stop-5BoxB (Addgene, #21301) using 'CTCGCTAGCCTCGAGGC TAGCTTCCCTAAGTC' and 'GACTCTAGACTCGAGATAATATCCTCGATAGGGCCCTTC' and subcloned into the pmirGLO (Promega) using EZ cloning kit (Enzynomics, EZ016S), resulting in pmirGLO-5XBoxB.

Recombinant TUT7 Purification

Human TUT7 cDNA region encoding amino acids 951-1,495 was cloned into a modified pRSF-Duet vector which has 6xHis and SUMO protein as an affinity tag at the N terminus. The fusion protein was overexpressed in *E. coli* BL21(DE3) cells in LB medium. The cells were induced when OD600 reached a value of 0.6 by 1 mM IPTG overnight in a shaker at 20°C. Protein was purified from the soluble fraction by a nickel-chelating affinity column, followed by overnight treatment of SUMO protease Ulp1 at 4°C to cleave the 6xHis-SUMO tag, which was later removed via a second nickel-chelating column. Protein was further purified by heparin chromatography followed by gel filtration chromatography using HiLoad 16/60 Superdex-200 preparative grade column (GE Healthcare) in buffer containing 20 mM Tris-HCl, pH 8.0, 150 mM NaCl and 1mM DTT.

Luciferase Assay and qRT-PCR

One day after seeding, HeLa cells grown in 24 well plates were transfected with 50 ng of pmirGLO-5XBoxB and 250 ng of HA-tagged or λN-HA-tagged protein expression plasmids using Metafectene (Biontex). Twenty four hours after transfection, cells were lysed and assayed by using Dual-Luciferase Reporter Assay (Promega) following manufacturer's instruction. Protein expression was confirmed by western blotting using anti-HA antibody (1:2,000, Santa Cruz, sc-7392) and anti-GAPDH antibody (1:2,000, Santa Cruz, sc-25778). Total RNA was prepared by using Maxwell 16 LEV simplyRNA Tissue kit (Promega, AS1280), treated with DNase I (Takara), and reverse transcribed by using RevertAid Reverse Transcriptase (Thermo Scientific, EP0442) and oligo(dT). Quantitative PCR was performed by using Power SYBR Green PCR master mix (Life Technologies, 4367659). The list of qRT-PCR primers is shown in Table S3.

Subcellular Fractionation

To isolate the cytoplasmic and nuclear fractions, ~5 × 10^6 HeLa cells were harvested and washed with cold PBS at 1,000 xg for 2 min at 4°C. After washing, cells were resuspended in 200 μl of lysis buffer (50 mM Tris [pH 7.4], 140 mM NaCl, 1.5 mM $MgCl_2$, 0.1% Igepal CA-630) and incubated on ice for 5 min. Centrifugation at 2,200 xg for 10 min at 4°C yielded the supernatant ("cytoplasmic" fraction). The remaining pellet was washed two times with wash buffer (50 mM Tris [pH 7.4], 140 mM NaCl, 1.5 mM $MgCl_2$) at 2,200 xg for 5 min at 4°C, followed by sonication and centrifugation at 16,000 xg for 15 min to collect the supernatant ("nuclear" fraction). The concentration of each fraction was measured by BCA assay (Pierce) and protein loading buffer was added to the lysate for western blotting.

Quantitative RT-PCR

Total RNA was extracted using TRIzol (Invitrogen), and 1–5 μg of total RNA was treated with DNase I (Takara), and reverse-transcribed by RevertAid Reverse Transcriptase (Thermo Scientific) and random hexamer. The mRNA levels were analyzed by SYBR green assays (Applied Biosystems) using ABI StepOne real-time PCR system. The list of primers used in qRT-PCR is shown in Table S3.

Western Blotting

Cells were lysed in 0.1% Triton X-100-Buffer D (200 mM KCl, 10 mM Tris-HCl [pH 8.0], 0.2 mM EDTA, 0.1% Triton X-100). 50 μg of each protein sample were separated on 6–10% SDS-PAGE gel and transferred to a methanol-activated PVDF membrane (GE Healthcare). The membrane was blocked for 1 hr in PBS-T containing 5% milk and subsequently probed with primary antibody for ~16 hr at 4°C. After washing three times with PBS-T, the membrane was probed with anti-mouse or anti-rabbit HRP-conjugated secondary antibodies (Jackson ImmunoResearch Laboratories). The protein was detected with West Pico Luminol reagents (Thermo Scientific) by using ChemiDoc XRS+ System (BioRad). Anti-TUT7 (1:500, Sigma, HPA020620), anti-TUT2 (1:500, Abcam, ab103884), anti-GAPDH (1:2,000, Santa Cruz, sc-32233), anti-Tubulin (1:1,000, Abcam, ab52866), anti-Lamin A/C (1:500, Santa Cruz, sc-6215), and anti-PABPC1 (1:1,000, 10E10, from Dr. G.Dreyfuss) were used as primary antibodies. Anti-TUT4 (1:500) polyclonal antibody was generated from rabbit.

FACS Analysis

HeLa cells were fixed in 70% cold ethanol and incubated in 4°C for overnight. Fixed cells were treated with RNase A (5 μg/ml) and stained with propidium iodide (50 μg/ml). Stained cells were analyzed for DNA content in FACSCanto (Becton Dickinson) using FACSDiva software.

T7 Endonuclease I Assay

T7E1 (T7 Endonuclease I) assays were carried out by ToolGen Inc. to detect DNA mutation introduced by CRISPR-Cas9. Genomic DNA was extracted from CRISPR-Cas9 treated cell pools or single colonies. The DNA fragment encompassing the targeted region was amplified by PCR, treated with T7E1 and resolved by agarose gel electrophoresis. Primer sequences are listed in Table S3.

SUPPLEMENTAL REFERENCES

Dobin, A., Davis, C.A., Schlesinger, F., Drenkow, J., Zaleski, C., Jha, S., Batut, P., Chaisson, M., and Gingeras, T.R. (2013). STAR: ultrafast universal RNA-seq aligner. Bioinformatics *29*, 15–21.

Quinlan, A.R., and Hall, I.M. (2010). BEDTools: a flexible suite of utilities for comparing genomic features. Bioinformatics *26*, 841–842.

Robinson, M.D., and Oshlack, A. (2010). A scaling normalization method for differential expression analysis of RNA-seq data. Genome Biol. *11*, R25.

Wu, T.D., and Nacu, S. (2010). Fast and SNP-tolerant detection of complex variants and splicing in short reads. Bioinformatics *26*, 873–881.

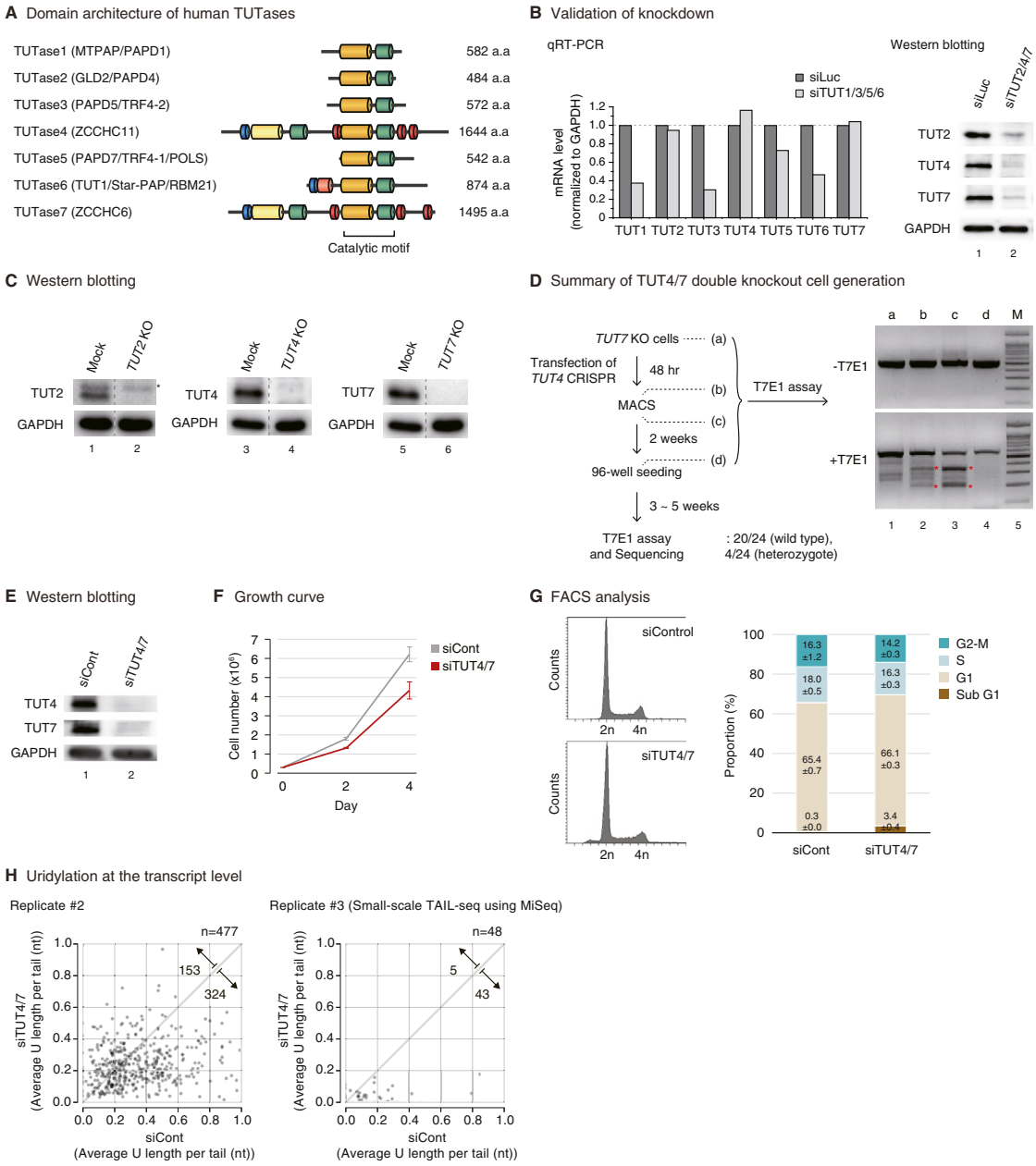

Figure S1. Confirmation of TUTase Depletion, Related to Figure 1

(A) Domain organization of human TUTases. Yellow, nucleotidyl transferase domain; green, PAP-associated domain; light yellow, inactive nucleotidyl transferase domain due to sequence variations; blue, C2H2 zinc finger domain; red, CCHC zinc finger domain; pink, RNA recognition motif.

(B) The level of seven TUTases after RNAi of TUT1/3/5/6 and TUT2/4/7, measured by qRT-PCR (left) and western blotting (right). GAPDH was used as a negative control in both qRT-PCR and western blotting.

(C) Validation of each knockout cell line by western blotting. An asterisk in TUT2 refers to a nonspecific band. Dashed lines indicate discontinuous lanes from the same gel.

(D) One of the unsuccessful attempts to generate TUT4/7 double knockout cell. *TUT7* KO HeLa cell was used as a parental cell line, and transfected with *TUT4* CRISPR-Cas9 to delete the *TUT4* gene. To detect mutation in genomic DNA, target region was amplified by PCR and T7E1 (T7 Endonuclease I) assay was carried out. T7E1 recognizes and cleaves heteroduplex formed between wild-type and mutated target sequence. "a to d" indicate the steps at which genomic DNA was extracted. (a) The parental *TUT7* KO cells, (b) before MACS (magnetic-activated cell sorting for enrichment of mutated clones), (c) right after MACS, and (d) 2 weeks after MACS. Red asterisks denote cleaved DNA fragments detected by T7E1 assay, which indicate that genomic deletions had been effectively introduced. 3–5 weeks after 96-well seeding, we analyzed 24 individual colonies. T7E1 negative clones were thought to be 'wild-type' clones. T7E1 positive clones were sequenced but all of them contained at least one wild-type allele for *TUT4* (heterozygote). Because none of the clones carried homozygous deletions for *TUT4*, our efforts to generate double knockout has failed despite the fact that the initial genomic deletion was successful. This indicates that double knockout of TUT4 and TUT7 may be lethal.

(legend continued on next page)

(E) RNAi to deplete TUT4 and TUT7 simultaneously by transfecting siRNAs into HeLa cells. The TUT4 and TUT7 protein levels were monitored by western blotting.
(F) Cell proliferation rates shown by cell counting. Cell numbers are presented as mean ± standard error of the mean (SEM) (n = 3).
(G) Cell cycle analysis. After 4 days of knockdown, cells were collected and profiled using BD FACSCanto and analyzed by BD FACSDiva software. (left) Cell cycle profiles. (right) The proportion of each cell cycle phase is displayed in stacked bar graph. The average percentages ± standard error of the mean (SEM) from three independent experiments are shown.
(H) Changes in uridylation at transcript level upon TUT4/7 knockdown. Average U length per tail (y axis) is the number of uridines on short A-tails (5–25 nt) divided by the total number of reads with short A-tails. Each dot represents a transcript with $\geq$ 15 reads in both samples. Replicate #3 was from "small-scale" TAIL-seq using Illumina MiSeq. Uridylation was significantly reduced when both TUT4 and TUT7 were knocked down ($p = 1.39 \times 10^{-15}$ for replicate #2, and $p = 1.38 \times 10^{-9}$ for replicate #3 by one-tailed Mann-Whitney U test).

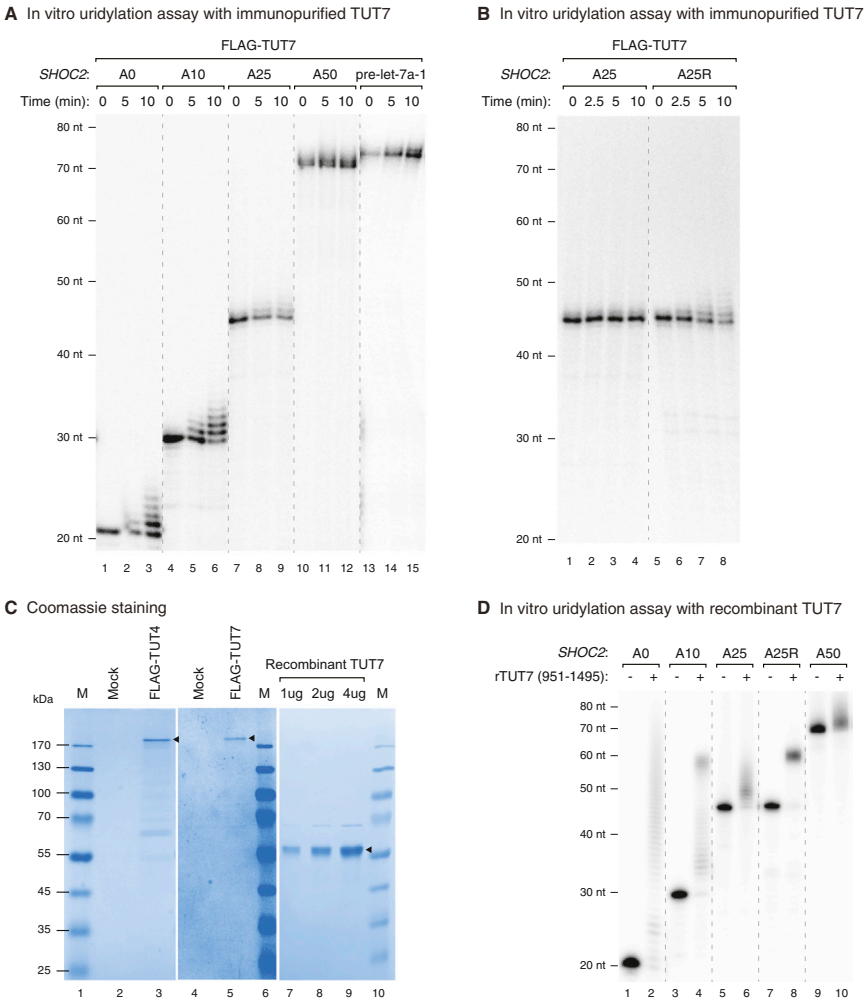

Figure S2. In Vitro Uridylation Assay by TUT7, Related to Figure 2

(A) In vitro uridylation assay using immunopurified full-length TUT7 and *SHOC2* RNAs (the same RNA substrates and reaction conditions as shown in Figure 2B). Dashed lines indicate discontinuous lanes from the same gel, which applies to all the dashed lines in the figure.

(B) In vitro uridylation assay using immunopurified full-length TUT7 and *SHOC2* RNAs (A25 and A25R). Uridylation efficiency for A25R was higher than A25. Reaction conditions are the same as in (A), except that the amount of TUT7 was smaller in (B) than in (A).

(C) Coomassie staining of immunopurified FLAG-TUT4 (full length), FLAG-TUT7 (full length), and recombinant TUT7 (951–1,495 aa) resolved on 10% SDS-PAGE gel. Each protein is indicated by an arrowhead. M, size marker.

(D) In vitro uridylation assay using recombinant TUT7 (951–1,495 aa) and *SHOC2* RNAs. 0.45 nM of RNA and 14 nM of recombinant TUT7 (rTUT7) were used in the reaction. Extension products were resolved on 12.5% polyacrylamide gel with 7 M urea.

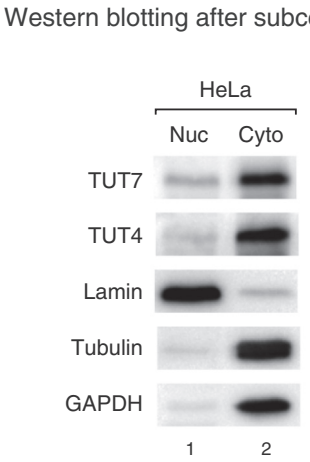

Figure S3. Subcellular Localization of TUT4/7, Related to Figure 3

Relative amount of TUT4 and TUT7 proteins in the nucleus and cytoplasm was measured by western blotting. Lamin was used as a nuclear marker while tubulin and GAPDH were used as cytoplasmic markers.

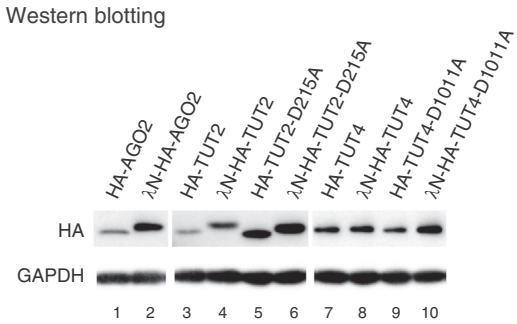

Figure S4. Protein Expression in the Tethering Experiment, Related to Figure 4

Western blotting showing the expression of transfected proteins in Figure 4C. GAPDH was used as a loading control.

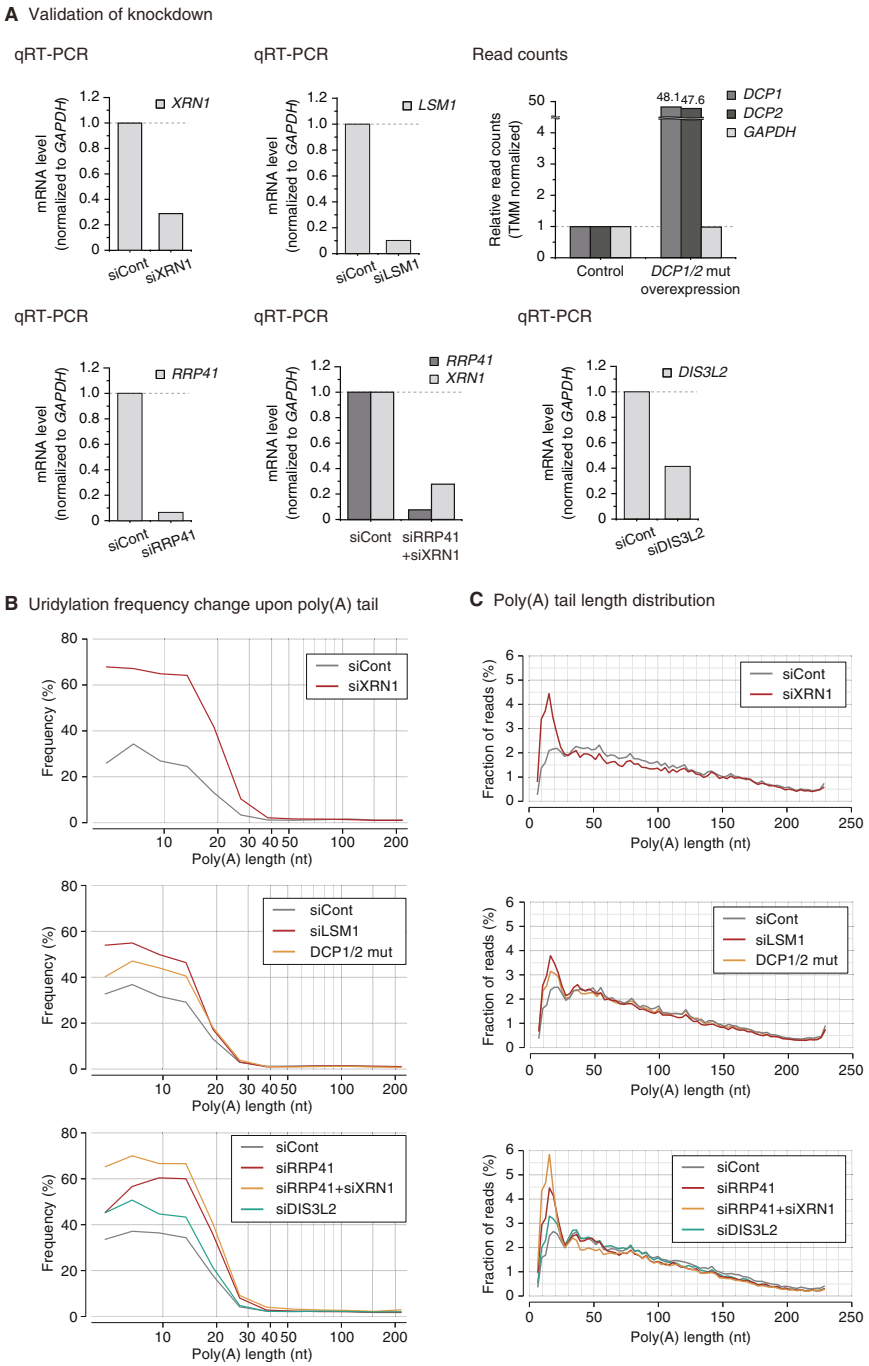

Figure S5. Inhibition of 5′-3′ and 3′-5′ Decay Factors, Related to Figure 6

(A) Validation of knockdown by qRT-PCR or sequencing. For the *DCP1/2* mutants overexpressed sample, the levels of *DCP1* and *DCP2* are shown in relative read counts (after trimmed mean of M values [TMM] normalized [Robinson and Oshlack, 2010]) from small-scale TAIL-seq experiments (with Illumina MiSeq). *GAPDH* was used as a negative control.

(B) Changes in uridylation frequency upon knockdown of decay factor(s). Poly(A) tail lengths from 5 nt to 231 nt are pooled into equal-width bins in a logarithmic scale (base 2) (x axis). The left edges (inclusive) of bins are 5, 7, 10, 14, 22, 33, 49, 74, 112, and 169 nt. Uridylation frequency (y axis) indicates the fraction of uridylated reads within each poly(A) tail size range.

(C) Global distribution of poly(A) tail length. Fraction of reads (y axis) shows the density of poly(A)$^+$ reads in each 3 nt bin.